Bulletin of the Seismological Society of America, Vol. 105, No. 3, pp. 1398–1418, June 2015, doi: 10.1785/0120140228

Earthquake Ground Motion in the Mygdonian Basin, Greece: The E2VP Verification and Validation of 3D Numerical Simulation up to 4 Hz

by E. Maufroy, E. Chaljub, F. Hollender,* J. Kristek, P. Moczo, P. Klin, E. Priolo, A. Iwaki,† T. Iwata, V. Etienne,‡ F. De Martin, N. P. Theodoulidis, M. Manakou, C. Guyonnet-Benaize, K. Pitilakis, and P.-Y. Bard

Abstract In a low-seismicity context, the use of numerical simulations becomes essential due to the lack of representative earthquakes for empirical approaches. The goals of the EUROSEISTEST Verification and Validation Project (E2VP) are to provide (1) a quantitative analysis of accuracy of the current, most advanced numerical methods applied to realistic 3D models of sedimentary basins (verification) and (2) a quantitative comparison of the recorded ground motions with their numerical predictions (validation). The target is the EUROSEISTEST site located within the Mygdonian basin, Greece. The site is instrumented with surface and borehole accelerometers, and a 3D model of the medium is available. The simulations are performed up to 4 Hz, beyond the 0.7 Hz fundamental frequency, thus covering a frequency range at which ground motion undergoes significant amplification. The discrete representation of material heterogeneities, the attenuation model, the approximation of the free surface, and nonreflecting boundaries are identified as the main sources of differences among the numerical predictions. The predictions well reproduce some, but not all, features of the actual site effect. The differences between real and predicted ground motions have multiple origins: the accuracy of source parameters (location, hypocentral depth, and focal mechanism), the uncertainties in the description of the geological medium (damping, internal sediment layering structure, and shape of the sediment-basement interface). Overall, the agreement reached among synthetics up to 4 Hz despite the complexity of the basin model, with code-to-code differences much smaller than predictions-to-observations differences, makes it possible to include the numerical simulations in site-specific analysis in the 3D linear case and low-to-intermediate frequency range.

Introduction: The EUROSEISTEST Verification and Validation Project (E2VP)

The estimation of site effects within the framework of a seismic-hazard study can involve different approaches, both empirical and numerical. However, in the context of low or moderate seismicity, the use of empirical approaches is difficult to implement due to the lack of representative earthquakes. Consequently, the application of numerical tools becomes essential. During the last decades, an important effort has been dedicated to develop accurate and computationally efficient numerical methods for predicting earthquake ground motion in heterogeneous media, especially in 3D (e.g., Moczo *et al.*, 2014). Henceforth, the progress in methods and the increasing capability of computers make it technically feasible to calculate realistic seismograms for frequencies of interest in seismic design applications (Kawase and Matsushima, 1998; Day *et al.*, 2001, 2003, 2005; Satoh *et al.*, 2001; Komatitsch *et al.*, 2004; Bielak *et al.*, 2010; Chaljub *et al.*, 2010).

However, before using the 3D ground-motion simulation codes for civil engineering design purposes, it is necessary to verify their accuracy and validate them for sedimentary basins (as they represent a typical situation for many important cities and critical facilities). Several international blind prediction tests were designed to compare numerical modeling methods and evaluate their capability to model earthquake ground motion in surface sedimentary structures. Beginning with the Turkey Flat, California (Cramer, 1995), and Ashigara Valley, Japan (e.g., Bard,

*Also at ISTerre, Univ. Grenoble Alpes, CNRS, IRD, IFSTTAR, BP 53, F-38041 Grenoble CEDEX 09, France.

†Now at National Research Institute for Earth Science and Disaster Prevention, 3-1 Tennodai, Tsukuba, Ibaraki 305-0006, Japan.

‡Now at Saudi Aramco, EXPEC Advanced Research Center. Dhahran, Saudi Arabia.

1992), blind tests focused on the effects of surface sediments; these were followed by the more comprehensive comparison exercises on the Osaka–Kobe basin area in Japan (Kawase and Iwata, 1998) and on the southern California area within the Southern California Earthquake Center (SCEC) framework (Day *et al.*, 2001, 2003, 2005; Bielak *et al.*, 2010), which also included the effects of extended sources and regional propagation in the low-frequency range. The Effects of Surface Geology 2006 (ESG2006) exercise focused on the Grenoble valley in the French Alps (Chaljub *et al.*, 2006, 2010; Tsuno *et al.*, 2006) and revealed that 3D numerical simulations were far from being a "press-button" tool. Among the lessons learned in this exercise, one was especially important for practical applications: predictions of the earthquake ground motion in complex geological structures should be made using at least two different but comparably accurate methods to enhance the reliability of the predictions. This conclusion is consistent with the well-known fact that no single method can indeed be considered as the best for all relevant medium-wavefield configurations (i.e., all important combinations of source characteristics and underground structures), in terms of accuracy and computational efficiency.

The ESG2006 exercise included only the verification of the numerical methods. We recall the concepts of verification and validation (e.g., Moczo *et al.*, 2014): verification of a numerical method may be defined as the demonstration of the consistency of the numerical method with the original mathematical–physical problem defined by the controlling equation, constitutive law, and initial and boundary conditions. The quantitative analysis of accuracy should be a part of the verification. Once the numerical method is analyzed and verified for accuracy, it should be validated using observations. In general, the validation may be defined as the demonstration of the capability of the theoretical model (i.e., the mathematical–physical model and its numerical approximation) to predict and reproduce observations.

The main motivation of the EUROSEISTEST Verification and Validation Project (E2VP) is a follow-up on this series of comparative exercises, with an extension to the validation part for the most advanced numerical modeling methods. E2VP is an international collaborative project (see Table 1), organized jointly by: the Aristotle University of Thessaloniki, Greece; the ITSAK (Institute of Engineering Seismology and Earthquake Engineering of Thessaloniki), Greece; the Cashima research project (supported by the French Alternative Energies and Atomic Energy Commission [Commisariat à l'énergie atomique et aux énergies alternatives, or CEA] and by the Laue-Langevin Institute [ILL], Grenoble); and ISTerre at Grenoble Alpes University, France. The E2VP target site is the Mygdonian basin near Thessaloniki, Greece, which is the international research and test site of many international seismological and earthquake-engineering projects. To foster the use of linear 3D numerical simulations in practical prediction, E2VP was designed to (1) evaluate the accuracy of the current most-advanced numerical methods when applied to realistic 3D models and (2) provide an objective, quantitative comparison between recorded earthquake ground motions and their numerical predictions. Part of the results obtained in these efforts is presented here.

Table 1
Teams and Institutions Contributing to the 3D Numerical Simulations of This Study

Institution	Country	Town	Team Acronym
Comenius University of Bratislava	Slovakia	Bratislava	CUB
Université Joseph Fourier	France	Grenoble	UJF
Disaster Prevention Research Institute, Kyoto University	Japan	Kyoto	DPRI
Istituto Nazionale di Oceanografia e Geofisica Sperimentale	Italy	Trieste	OGS
Université de Nice, Sophia Antipolis	France	Valbonne	UNICE
Bureau de Recherches Géologiques et Minières	France	Orléans	BRGM

The article is accompanied by the methodological study of Chaljub *et al.* (2015). It focuses on quantitative and qualitative analysis of accuracy (i.e., verification) of four numerical modeling methods in their application to stringent canonical models directly related to the model of the Mygdonian basin.

The Target Site: The Mygdonian Basin, EUROSEISTEST, Greece

The first step of E2VP was to identify a suitable test site, that is, a site coupling a good preexisting geological, geophysical, and geotechnical characterization with a sufficient number of available recordings from adequately deployed seismic stations. Such conditions are rarely fulfilled within the Euro-Mediterranean area, and the selection process resulted in decision for the EUROSEISTEST site, located 30 km east-northeast of Thessaloniki, northeastern Greece (see Fig. 1).

The site is located at the center of the Mygdonian sedimentary basin between the Volvi and Lagada lakes, in the epicentral area of the magnitude 6.5 event that occurred in 1978 and damaged the city of Thessaloniki. The Mygdonian basin has been extensively investigated within the framework of various European projects (Pitilakis *et al.*, 2009). A detailed 3D model is available based on works by Manakou *et al.* (2007, 2010). Dense instrumentation, including surface accelerometers (Fig. 1) and a vertical array of six sensors spread over a depth of about 200 m at the central TST site, produced numerous accelerograms (Pitilakis *et al.*, 2013).

The basin has been shaped by north–south extensive tectonics, with east–west-trending normal faults on each side. The velocity structure of the basin is well constrained along the central north-northwest–south-southeast profile crossing

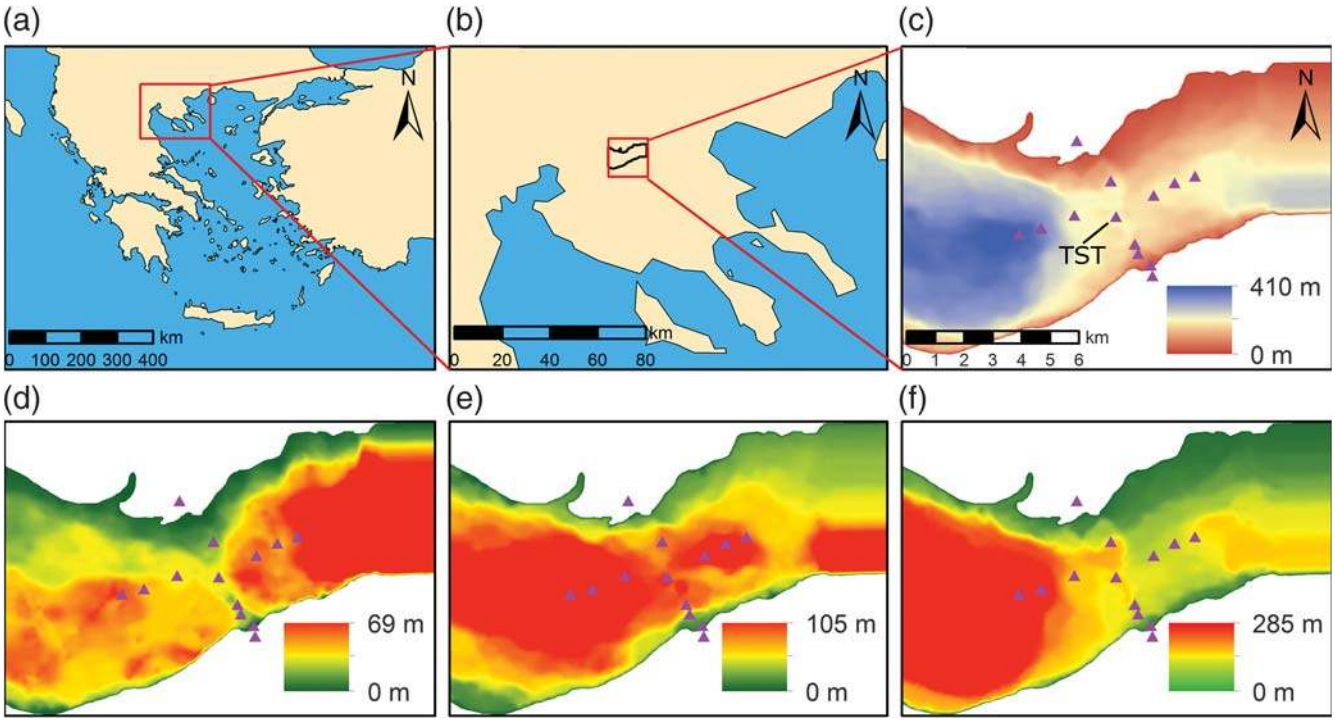

Figure 1. (a,b) Location of the EUROSEISTEST site within the Mygdonian basin in northeastern Greece; (c) total sediment thickness in the basin; thicknesses of (d) shallow layer 1 in the 3D model, (e) layer 2, and (f) deep layer 3 (see Table 2). Note the strong lateral variations and the asymmetries between the northern and southern edges, as well as between the western and eastern sides. The location of the EURO-SEISTEST accelerometric array is represented by the purple triangles. The central accelerometric site TST appears as a saddle point, with a maximum of sediment thickness along a north–south profile and a minimum along an east–west profile.

the central TST site, based on a large number of geophysical and geotechnical measurements, surface and borehole seismic prospecting, electrical soundings, and microtremor recordings (Jongmans *et al.*, 1998; Raptakis *et al.*, 2000). Along that profile, the sediment thickness reaches its maximum at the TST site (196 m), and the *S*-wave velocity (V_S) increases from 130 m/s at the surface to about 800 m/s at a large depth. Because the velocity in the underlying bedrock is 2600 m/s, the velocity contrast at the sediment–bedrock interface is large. The 3D structure in the whole graben has been extrapolated from the central profile, taking into account information from many single-point microtremor measurements, array microtremor recordings, one east–west refraction profile, and old deep boreholes drilled for water exploration purposes (Raptakis *et al.*, 2005). The resulting detailed 3D model of the basin (Manakou, 2007; Manakou *et al.*, 2007, 2010) is 5 km wide and 15 km long, with the maximum sediment thickness reaching about 410 m. The TST site resembles a saddle point, with the sediment thickness increasing both eastward and westward, off the north-northwest–south-southeast central profile, which actually corresponds to a buried pass between two thicker sub-basins (Fig. 1). The slope of the northern basin edge is much gentler than the steep slope of the southern edge: the meshing of the 3D model thus requires specific attention and care, as the diffraction on the longer northern basin edge is very efficient. The whole area presents a rather smooth topography: a preliminary sensitivity study indicated only negligible impacts on ground motion (waveforms and engineering parameters), and it was decided to not include the topography in the main E2VP simulations. It was flattened, changing the elevation of each interface but keeping unchanged the local thickness of the various layers.

The mechanical properties of the 3D models are given in Table 2. We used two different velocity models (A and B). Realistic model A consists of three sediment layers with laterally varying thicknesses, according to the propositions by Manakou *et al.* (2007, 2010). Within these three layers, properties are constant (homogeneous). Model B keeps exactly the same geometry but replaces the homogeneous layers with increasing-velocity linear gradients to avoid any internal velocity jumps within the sedimentary filling. Model B is a smoothed version of model A and was designed only for the verification purposes of this study. Outside the basin, the crustal 1D velocity model of Papazachos (1998) has been considered for the regional propagation. The attenuation is assumed to be correctly represented by a frequency-independent quality factor Q and a reference frequency of 1 Hz.

Some features of the models deserve a special mention because of their impact on the difficulty of the numerical simulations: (1) the simultaneous existence of a soft shallow layer and of a high water table, with $V_S = 200$ m/s and *P*-wave–to–*S*-wave velocity ratio $V_P/V_S = 7.5$, and (2) a very hard bedrock leading to large impedance contrast and effi-

Table 2
Mechanical Properties of the Two 3D Models Used in the Present Study

Model	Layer	V_S (m/s)	V_P (m/s)	ρ (kg/m3)	Q_S	Q_κ
Layered model A (constant properties within layers)	1	200	1500	2100	20	∞
	2	350	1800	2200	35	∞
	3	650	2500	2200	65	∞
Smooth model B (linear increasing gradient within layers)	1	200–250	1500–1600	2100	20–25	∞
	2	250–500	1600–2200	2100–2130	25–50	∞
	3	500–900	2200–2800	2130–2250	50–90	∞
Bedrock		2600	4500	2600	260	∞

In layered model A, each layer has homogeneous properties but laterally varying thickness. Smooth model B is built with linear velocity gradients and without any discontinuity within the sediments. Model B is designed only for verification purposes and is therefore not used in the validation (model A being the realistic model). V_S, *S*-wave velocity; V_P, *P*-wave velocity; ρ, mass density; Q_S, shear quality factor; and Q_κ, bulk quality factor. The Q values are assumed to be frequency independent.

cient wave trapping. Model details were defined for a maximum simulation frequency of 4 Hz.

How to Objectively Quantify the Similarity between Two Signals?

There are many ways to compare two seismograms in the time or frequency domain: each depends on the quantities to be compared (from the whole signal to selected engineering parameters) and on the method used to compute the differences between quantities. Recently, Kristeková *et al.* (2006, 2009) developed misfit criteria based on the time–frequency (TF) representation of the seismic signals using the continuous wavelet transform with the Morlet wavelet. Provided the signals under comparison are not too different, the TF misfit criteria are sensitive either to differences in envelope (amplitude) or in phase. The TF misfit criteria are therefore particularly well suited for the comparison of numerical synthetics (computed for the same models with different methods), and they allow a proper characterization of the nature of the differences between seismograms.

As is well known, waveform differences between earthquake records and their numerical predictions can be relatively large; however, an objective and quantitative way of comparing signals is necessary. From an engineering viewpoint, Anderson (2004) proposed characterizing the similarity between two seismograms by a goodness-of-fit (GOF) based on 10 ground-motion parameters commonly used in earthquake engineering: the peak acceleration, peak velocity, peak displacement, Arias intensity, the integral of squared velocity, Fourier spectrum and acceleration response spectrum on a frequency-by-frequency basis, the shape of the normalized integrals of acceleration and velocity squared (Husid plots), and the cross correlation. The investigated frequency range can be split into narrow frequency subintervals to be evaluated separately. The agreement between the two compared seismograms is quantified on each parameter by a GOF value between 0 and 10, with 10 meaning perfect agreement. Anderson (2004) also introduced the following verbal scale for GOF: a score below 4 is a poor fit, a score of 4–6 is a fair fit, a score of 6–8 is a good fit, and a score over 8 is an excellent fit. The Anderson GOF may be considered a robust criterion for comparing recordings with their numerical predictions.

Considering the somewhat redundant character of some components of the original Anderson parameters, we restricted our comparison in the present study to five parameters. Three of them are representative of the signal amplitude in different frequency bands: peak value of the acceleration time series (peak ground acceleration [PGA], C1); spectral acceleration at intermediate frequencies (around 2 Hz, C2); and spectral acceleration at lower frequencies (around 0.5 Hz, C3). The other two are representative of the total amount of energy contained in the signal (cumulative absolute velocity [CAV], C4) and of the duration (relative significant duration [RSD], C5). Arguments for the selected characteristics and details on their computations are provided in the Appendix. For these five ground-motion parameters, the direct misfit between two signals is quantified in percentage. The misfit value is positive when the prediction overestimates the target (or reference) signal, and negative when the prediction underestimates the target signal.

In this article, we also follow the GOF procedure by Kristeková *et al.* (2009) that describe the envelope and phase GOF criteria based on the TF misfit criteria. Thus, we consider the GOF as

$$\mathrm{GOF} = 10\exp(-|M|), \tag{1}$$

in which M represents a single-valued misfit in the envelope or phase. GOF ranges from 0 (no fit) to 10 (perfect fit); further details may be found in Kristeková *et al.* (2009): to summarize, a GOF value of 8 corresponds to a misfit of 20%, and a GOF value of 6 to a misfit of 50%. The TF-based GOF values are considered only in the verification part of E2VP, as the numerical predictions are sometimes too different from the actual recordings.

Verification: Cross-Comparisons between Various 3D Numerical Predictions of Ground Motion in the Mygdonian Basin

Several teams contributed to the verification phase of E2VP. They used a variety of methods or implementations of the same method: finite-difference method (FDM), Fourier

Table 3
Applied 3D Methods Used by the EUROSEISTEST Verification and Validation Project (E2VP) Participants to This Study

Team and 3D Acronyms	Method	Characterization	Attenuation	Absorbing Boundary Conditions	References
CUB 3D01	FDM	Finite difference, fourth-order velocity-stress volume arithmetic and harmonic averages of density and moduli, arbitrary discontinuous staggered grid	GZB 4 relaxation mechanisms	CPML	Kristek *et al.* (2002, 2010); Moczo *et al.* (2002, 2004, 2014)
UJF 3D02	SEM	Spectral element, Legendre fourth-order polynomial Gauss–Lobatto–Legendre integration	GZB 3 relaxation mechanisms	Stacey (1988)	Chaljub *et al.* (2007); Peter *et al.* (2011)
DPRI 3D03	FDM	Finite difference, fourth-order velocity-stress nonuniform staggered grid	linear $Q(f)$ $f_0 = 2$ Hz, Graves (1996)	Clayton and Engquist (1977) A1 + Cerjan	Pitarka (1999)
OGS 3D04	FPSM	Fourier pseudospectral, vertically stretching staggered grid	GZB 3 relaxation mechanisms	CPML	Klin *et al.* (2010)
UNICE 3D09	DGM	Discontinuous Galerkin, velocity-stress second-order Lagrangian polynomials with tetrahedral mesh and homogeneous physical properties within elements	n.a.	CPML	Etienne *et al.* (2010)
BRGM 3D11	SEM	Spectral element, Legendre fourth-order polynomial Gauss–Lobatto–Legendre integration	Memory variables with eight relaxation mechanisms	Stacey (1988) paraxial P1 approximation	De Martin (2011)

All methods are second-order in time. GZB, generalized Zener body; CPML, convolutional perfectly matched layer (Martin and Komatitsch, 2009); n.a., not applicable. See also Data and Resources.

pseudospectral method (FPSM), spectral-element method (SEM), and discontinuous Galerkin method (DGM). Additional details on each method can be found in Tables 1 and 3.

In what follows, we compare the 3D ground-motion simulations obtained with each code for a virtual M_w 1.3 event occurring beneath the Mygdonian basin, considering both the layered model A and the smooth model B (Table 2). A double-couple point source is assumed at 5 km depth beneath the TST central site (blue star in Fig. 2), with normal faulting to match the typical regional focal mechanism (strike, 260°; dip, 40°; rake, −90°); the source time function is a Heaviside step function low-pass filtered below 3 Hz with a 10-pole causal Butterworth filter. For each source-model configuration, the teams were required to simulate 30 s of ground motion at 287 receivers (yellow triangles in Fig. 2). The required frequency range up to 4 Hz was intended to cover the low-to-intermediate frequencies at which ground motion is significantly affected by the basin.

Layered Model with Attenuation

Figure 3a shows velocity seismograms at the central TST site simulated by five teams for the layered model A, including attenuation. Note the good agreement of all numerical predictions at early arrivals (less than 6 s), especially on the vertical component, and the large differences in phase and amplitude at late arrivals. Some of those differences, in particular in the amplitude of the later arrivals, are attributed to the fact that the method of team 3D03 applies a frequency dependence of Q: it approximates the required model value only near the reference frequency f_0, and an almost linear increase of Q with frequency is applied above f_0, whereas other teams modeled the required constant Q. Globally, the numerical predictions by teams 3D01, 3D02, 3D04, and 3D11 are very close in the whole time window.

Figures 4 and 5 show maps of the envelope and phase GOFs (equation 1) evaluated at the virtual receivers for numerical predictions by teams 3D01, 3D02, 3D03, 3D04, and 3D11. The GOF values are evaluated in the 0.5–4.0 Hz frequency range as the weighted average for the horizontal components of the ground velocity in Figure 4 and for the vertical component in Figure 5. "Weighted average" means that the larger component is given a proportionally larger weight; such a weighting was considered to avoid meaningless values corresponding to large relative differences on very weak components (for instance on rock near the nodal planes). Each small colored circle represents a value of GOF between numerical predictions by two teams for the corresponding receiver. The color scale ranges from an extremely poor fit (red) to an excellent fit (blue). The GOF maps are useful in tracking differences between numerical predictions. Table 4 summarizes the weighted averages (with the same amplitude-dependent weighting) of GOF evaluated for rock and soil (sedimentary) sites for the investigated verification cases. Figure 4 and Table 4 show that the results obtained by teams 3D01, 3D02, 3D04, and 3D11 for layered model A with attenuation are the most similar, with GOF values in the basin mostly comprised between 6 and 8 (good fit). Outside the basin, the GOF values rise above 8 (excellent fit) at the rock sites.

The smaller values of GOF between the 3D03 and other synthetics are mainly due to the differently implemented attenuation. The GOF values for the basin are mostly between 4 and 6 (fair fit) but fall under 4 for some central receivers. The level of agreement is smaller for envelopes. This is understandable: the attenuation mostly affects the amplitudes of the waveform.

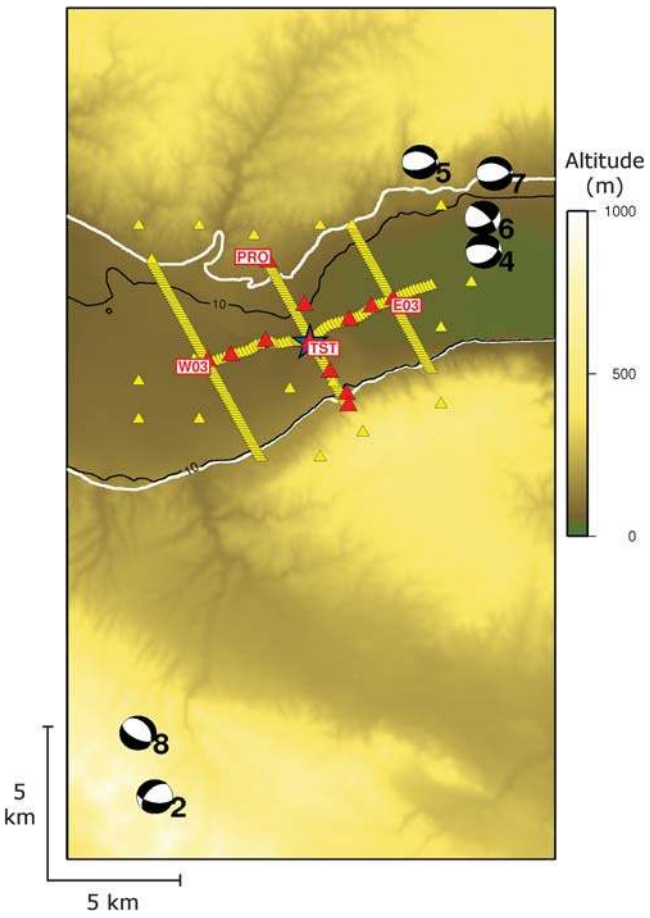

Figure 2. Detailed locations of the virtual central source (epicenter at the blue star) and of the six local real events (beachballs with event numbers) selected for the EUROSEISTEST Verification and Validation Project (E2VP) validation exercise and recorded by the EUROSEISTEST accelerometric network (red triangles), superimposed to the virtual receivers (yellow triangles) considered in the E2VP verification exercise. The white line denotes the basin edge, and the black line is the location where the sediment thickness equals 10 m. The background color scale corresponds to the free-surface elevation.

Layered Model without Attenuation

We next consider the case of the layered model A without attenuation to remove the differences caused by the implementation of attenuation. Consequently, the eventual differences should be mainly due to the discrete representation of material heterogeneities, to the numerical dispersion, and to spurious reflections from the boundaries of the numerical grid. Especially, the discrete representation and dispersion can considerably affect the solutions because locally generated surface waves propagate over relatively long distances in the perfectly elastic medium. The velocity seismograms at the central TST site simulated by the five teams are shown in Figure 3b. Dispersive surface waves dominate the waveforms. Large differences (in phase and amplitude) are observed on late arrivals (after 6 s), corresponding partly to surface waves diffracted off the valley edges and traveling toward the center of the basin without being attenuated.

Figure 6 shows the maps of envelope and phase GOFs (weighted average over the three components of ground velocity) between the numerical predictions by teams 3D01, 3D02, 3D03, 3D04, and 3D09. The overall level of GOFs is lower compared to the case with attenuation (see also the average GOF values for soil sites in Table 4). The general decrease of fit between the numerical predictions is mainly due to the large differences in late high-frequency arrivals, which are not attenuated compared to the case with attenuation. The phase GOF values are smaller than the amplitude GOFs: the numerical dispersion mostly affects the short-wavelength waves traveling over long distances.

Smooth Model without Attenuation

The presence of material interfaces in sediments in the layered model A certainly affects the generation and propagation of surface waves in sediments. The role of the material interfaces was pointed out by comparing the numerical predictions for the layered model A with and without attenuation. It is thus reasonable to include another comparison. The smooth model B has the same geometry of interfaces within sediments as the layered model A, but material parameters do not change at these interfaces. What changes at the interfaces is just the gradient (see the mechanical properties in Table 2). This is achieved by linear variations of parameters with depth inside layers.

Figure 3c shows the velocity seismograms at the central site TST, simulated in the smooth model B by teams 3D01, 3D02, 3D04, and 3D09. The similarity of the seismograms, including parts with surface-wave packets arriving at late times, is striking. The maps of the GOF values for the available predictions are shown in Figure 7, and the associated weighted average GOFs are given in Table 4 (see above for the weighting scheme). Compared to the GOF maps in Figure 6 for the elastic layered model A, it is clear that globally the GOF values for the smooth model B are considerably higher (see also Table 4 for the soil sites). Indeed, the GOF values obtained for the smooth model B are mostly above 6 in the basin and often rise above 8, whereas GOF values for the layered model A are one level lower (mostly above 4, often above 6, but almost all under 8). It is also noteworthy that the GOF values for the elastic smooth model B are larger than the GOF values for the layered model A with attenuation (compare Figs. 7 and 4). Material interfaces at which material parameters change discontinuously are thus clearly identified as one key factor that significantly affects the accuracy of the 3D numerical simulations. In other words (and from the optimistic viewpoint), it is not difficult to reach a very good level of agreement for the sedimentary basin with smooth variations of material parameters.

Discussion on the Comparison Criteria

Figure 8 displays the absolute values of misfits evaluated for the selected engineering criteria (C1–C5; see the Appendix) as a function of the GOF values evaluated according to equation (1) for the three basin models and for teams 3D01, 3D02,

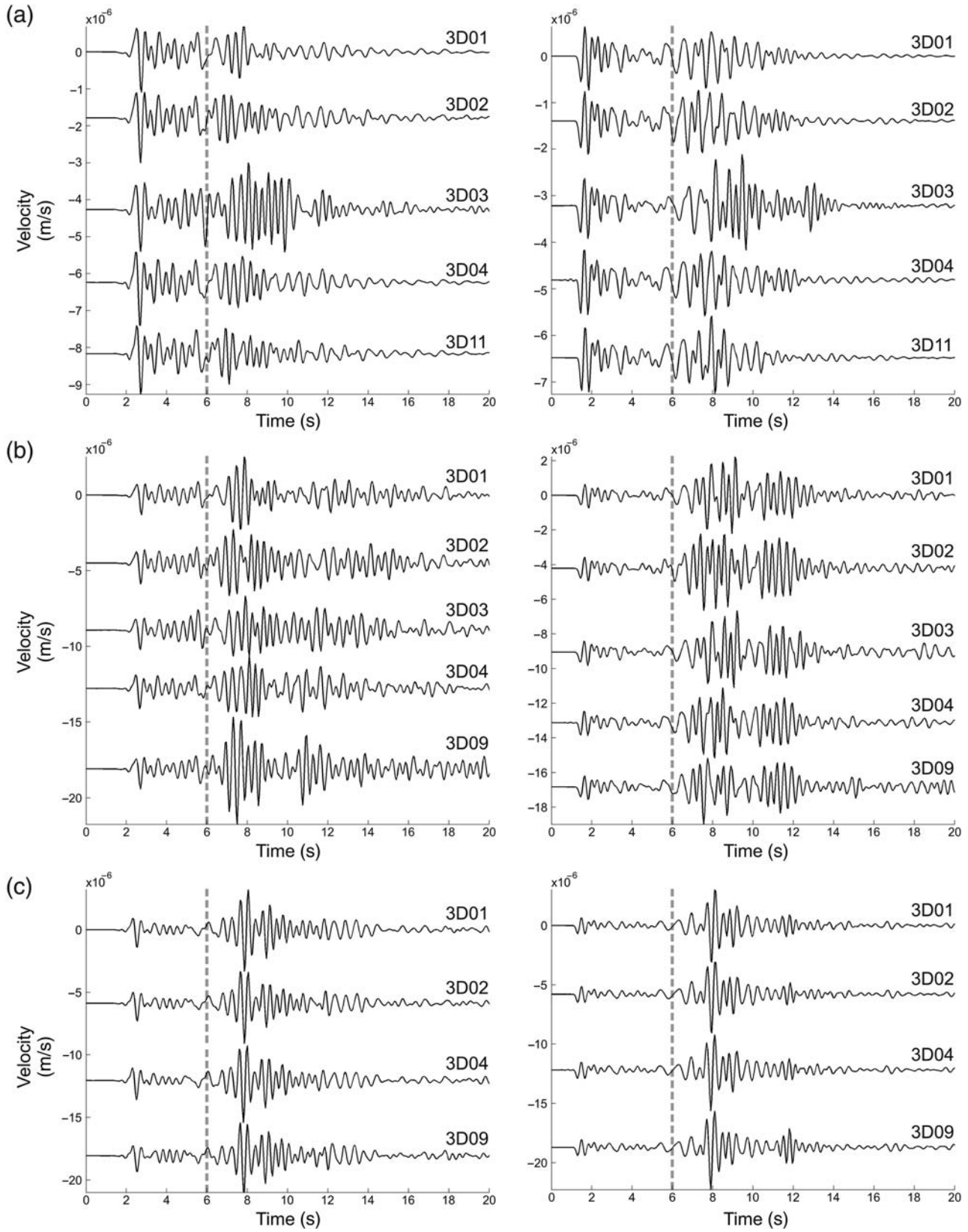

Figure 3. North–south (left) and vertical (right) components of synthetic ground velocity at central soil site TST, computed by four or five different teams for a virtual central event in three cases: (a) the viscoelastic simulation in layered model A, the pure elastic simulation in (b) the layered model A, and (c) the smooth model B. Most of the numerical predictions are consistent for the first 6 s, before the arrival of the later phases, among which surface waves diffracted off the valley edges. Note that team 3D03 did not implement the requested constant-Q viscoelastic rheology.

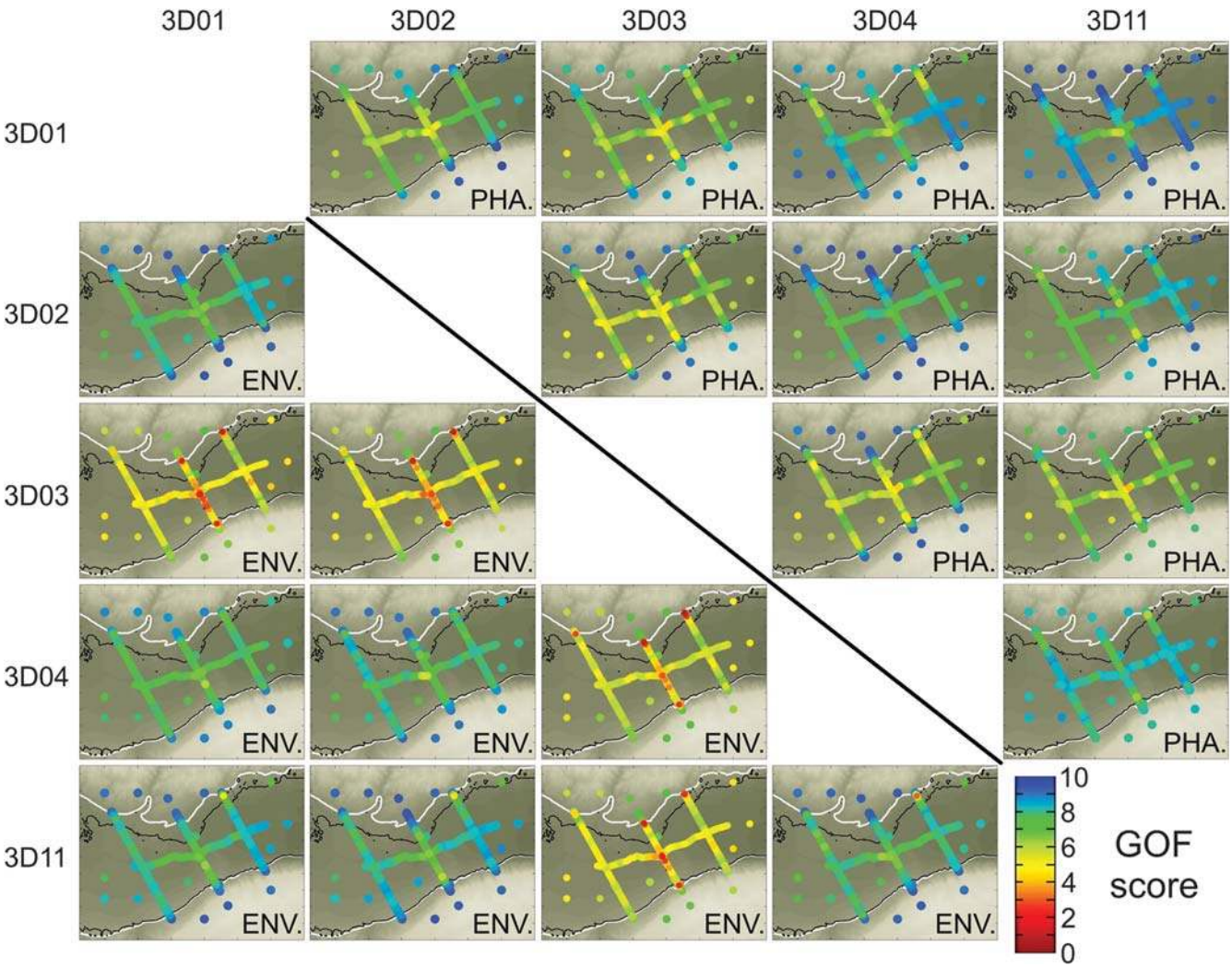

Figure 4. Locations of goodness-of-fit (GOF) values (following the GOF procedure by Kristeková *et al.*, 2009) for the viscoelastic rheology case in the layered model A of the Mygdonian basin. The scores are computed as the weighted average (see the Layered Model with Attenuation section) over both horizontal components of ground velocity for five different numerical predictions (by teams 3D01, 3D02, 3D03, 3D04, and 3D11). The bottom left block of plots displays the envelope scores (ENV.); the upper right block displays the phase scores (PHA.). Each colored dot corresponds to the envelope (amplitude) or phase GOF value computed in the whole frequency range (0–4 Hz) at the corresponding virtual receiver. Score 0 (red) corresponds to a very poor fit between the two numerical predictions of two teams, whereas score 10 (blue) corresponds to a perfect fit. The results of one team relative to the other teams are to be found on the line and column labeled by the team 3D acronym.

3D04, 3D09, and 3D11. We can see a very satisfactory relationship between the misfits (except for criterion C5) and GOFs: when a GOF decreases, the corresponding misfit increases. It is also clear that in terms of C1–C5 misfit criteria, the numerical predictions by all teams for the three models are close: no misfit exceeds 30% and most of them are below 20%. In particular, the misfits for the smooth model B are clearly lower than the misfits for the layered model A. We also see, as expected, a clear difference between the rock and soil sites: the level of agreement at the rock sites is significantly better (excellent in the GOF verbal classification) than at the soil sites for all the three models and for each criterion but C5.

The misfit for criterion C5 (RSD) correlates well with the GOF at the soil sites (solid symbols in Fig. 8), but a different trend appears at the rock sites (empty symbols in Fig. 8): the C5 misfit indicates disagreement, whereas the corresponding GOFs are all above 8 (excellent agreement). The higher C5 misfits at the rock sites are due to the fact that a small difference in duration between two signals gives a high misfit in percentage if the duration of the target signal is short. For example, the average signal durations in the elastic smooth model B (green symbols in Fig. 8) are equal to 1.34 s (team 3D01) and 0.99 s (team 3D02) at rock sites, whereas they increase to 18.07 s (3D01) and 18.29 s (3D02) at the soil sites. The average differences in duration between the numerical predictions of these two teams are equal to 0.36 s for the rock sites and 0.68 s for the soil sites. These differences are of the same order, but the relative misfits in percentage are higher at the rock sites (18.8%) where the duration is short compared to the longer duration at the soil sites (5.4% of misfit).

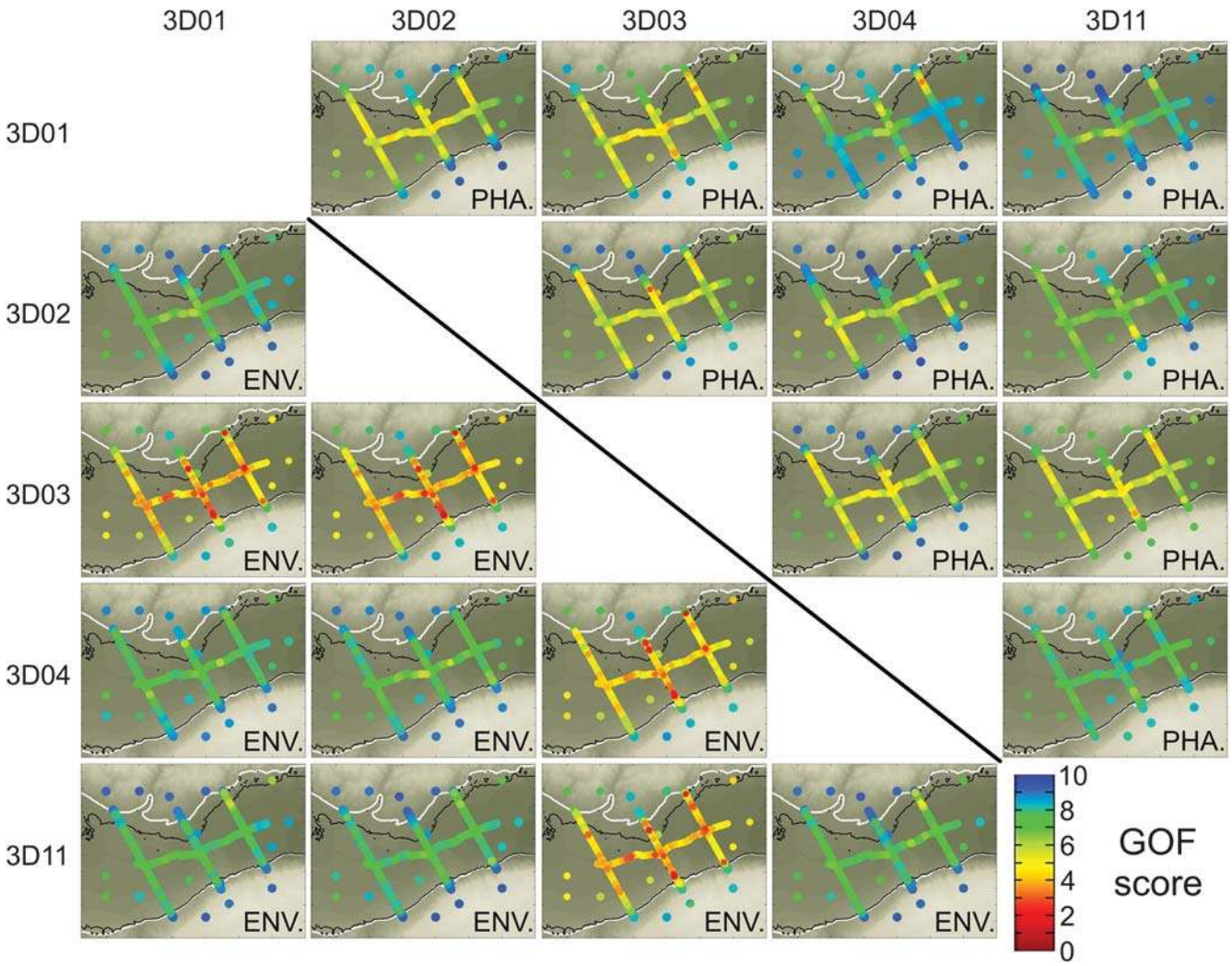

Figure 5. Same as Figure 4, but for the vertical component.

Table 4

Summary of Goodness-of-Fit (GOF) Values (Following the GOF Procedure by Kristeková *et al.*, 2009) Obtained for the Three Verification Cases Presented in This Article

		Receivers at Rock Sites				Receivers at Soil Sites			
		H component		*V* component		*H* component		*V* component	
		Env.	Ph.	Env.	Ph.	Env.	Ph.	Env.	Ph.
Layered model A, with *Q*	3D01–3D02	9.3	8.7	9.2	8.8	8.0	7.0	7.6	5.8
	3D01–3D03	6.6	8.2	8.1	8.2	5.6	6.9	4.8	5.8
	3D01–3D04	8.8	8.6	8.8	8.7	7.8	7.8	7.9	7.4
	3D01–3D11	9.2	9.5	9.2	9.3	8.1	8.6	8.0	8.0
Layered model A, no *Q*	3D01–3D02	9.2	8.8	9.0	8.8	6.7	5.6	6.5	4.5
	3D01–3D03	8.0	7.4	7.8	7.6	6.5	6.2	6.4	5.5
	3D01–3D04	8.7	8.2	8.7	8.3	6.6	4.9	6.2	4.7
	3D01–3D09	9.3	8.7	9.1	8.6	6.3	5.1	5.9	4.8
Smooth model B, no *Q*	3D01–3D02	9.6	9.6	9.3	9.5	8.2	8.4	8.2	8.6
	3D01–3D04	9.6	9.6	9.4	9.6	8.0	8.2	8.2	8.0
	3D01–3D09	9.6	9.6	9.3	9.4	7.8	7.4	7.6	7.1

The scores are given in envelope (Env.) and phase (Ph.) for each team relative to team 3D01. The values are weighted averages computed either on 19 rock sites or on 268 soil sites (weighting individual GOF values by the corresponding time–frequency amplitude to emphasize the GOF values of the most energetic points).

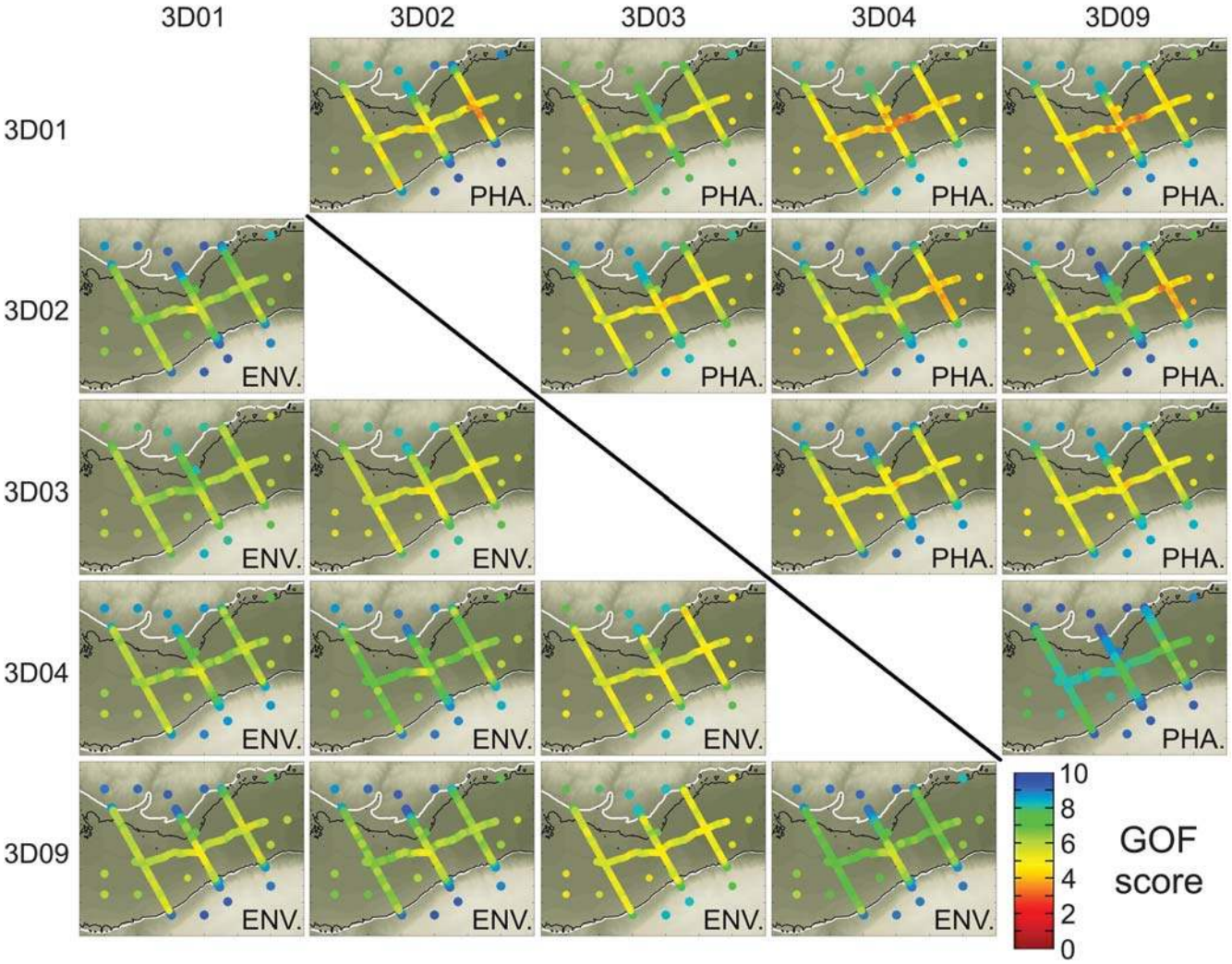

Figure 6. Same as Figure 4, but without attenuation. The scores are computed as the weighted average (see the Layered Model with Attenuation section) over the three components of ground velocity for five different numerical predictions (by teams 3D01, 3D02, 3D03, 3D04, and 3D09).

Based on these comparisons and analyses, we conclude that the selected ground-motion characteristics C1–C5, which are more relevant for earthquake-engineering purposes, make a reasonable and acceptable alternative to the GOFs (equation 1) for comparing dissimilar waveforms. We will thus use them for the validation phase (next section) to quantitatively compare recorded waveforms with their numerical predictions.

An Overall Evaluation

As already pointed out and clearly appearing in Figure 3, the velocity seismograms obtained by different teams differ from each other mostly for the layered model A without attenuation (with the exception of the 3D03 solution for model A with attenuation, due to their different implementation of the attenuation, as discussed previously). These differences among synthetics are well reflected by GOFs based on the TF misfits (equation 1). The selected (earthquake-engineering) criteria, as expected, provide a robust and different view on the level of agreement among the synthetics for the layered model A with and without attenuation. The C4 (CAV) misfits are relatively low for model A without attenuation, whereas the C5 (RSD) misfits are relatively low for model A with attenuation (see Fig. 8). The attenuation eventually improves prediction of the signal duration in the basin sediments.

Overall, given the complexity of the Mygdonian basin model, the level of similarity of all the 3D simulations up to 4 Hz (a rather high frequency with wavelengths as short as 50 m) is encouraging.

On the other hand, the verification phase of E2VP confirmed the previous experience of the ESG2006 comparative exercise for the complex model of the Grenoble valley (Chaljub *et al.*, 2010). Cross comparisons among methods and iterations (to remove technical errors and possibly to improve the method or code) are still necessary for a reliable numerical prediction of ground motion in complex models.

The discrete representation of continuous and discontinuous material heterogeneity, the attenuation model, the

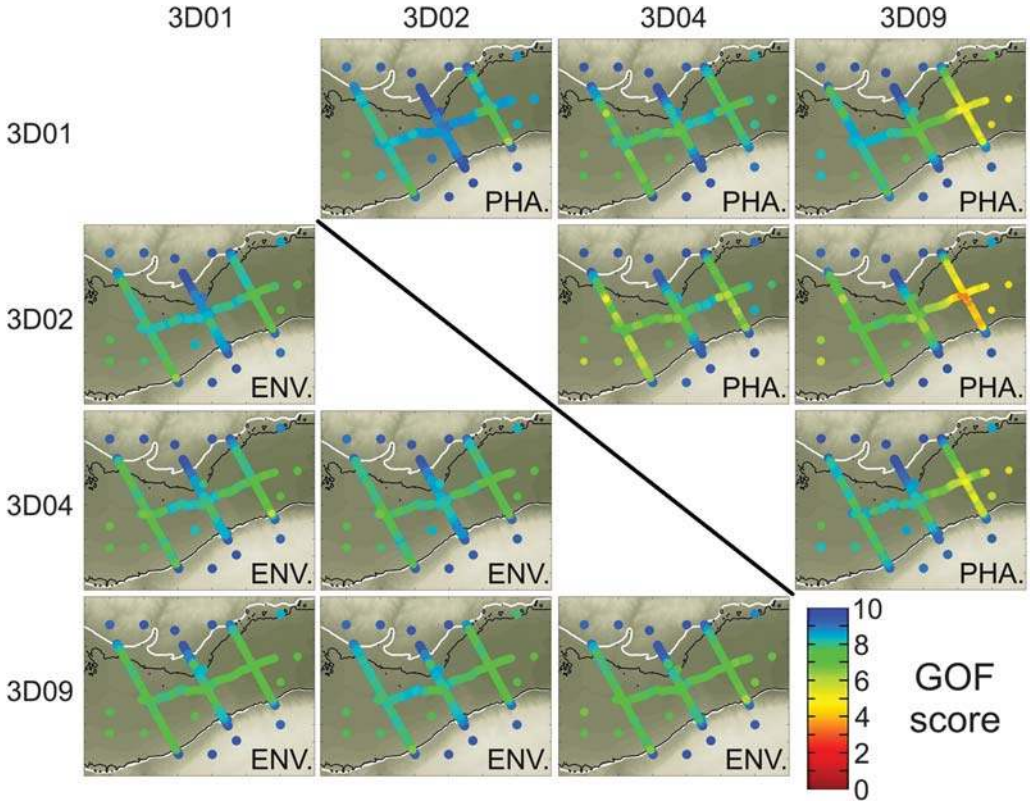

Figure 7. Same as Figure 4, but for the smooth model B, without attenuation. The scores are computed as the weighted average (see the Layered Model with Attenuation section) over the three components of ground velocity for four different numerical predictions (by teams 3D01, 3D02, 3D04, and 3D09).

approximation of the free surface, and nonreflecting boundaries are identified as the main sources of differences among the numerical methods and/or codes. All of those key elements need proper implementation in the methods and codes for a sufficiently accurate simulation of ground motion at sites atop complex local sedimentary structures. A more detailed discussion of these factors and the way to reduce the related code-to-code differences are provided by Chaljub *et al.* (2015).

Implementation of attenuation into the 3D numerical simulations has a complex impact on the accuracy of the numerical predictions (e.g., compare the C4 and C5 misfits in Fig. 8). Importantly, a proper attenuation model apparently improves the level of agreement among different predictions in the sedimentary basin, as waveforms are not dominated by strong late arrivals of very dispersive surface waves.

Besides the attenuation, a smooth velocity distribution inside sediments allows reaching significantly improved levels of agreement among different predictions.

In conclusion of the verification phase, the encouraging level of agreement among numerical predictions up to 4 Hz, the subsequent identification of the factors affecting the accuracy of the simulations, and indications for correct handling of those factors (Chaljub *et al.*, 2015) support the use of the 3D numerical modeling approach for predicting ground motion, at least in the linear, low-to-intermediate frequency range, and provided it is performed wisely and carefully.

Validation: Comparison of 3D Numerical Predictions with Earthquake Recordings in the Mygdonian Basin

The next phase in E2VP is the validation part, consisting of a quantitative comparison between numerical predictions and actual recordings in the frequency range up to 4 Hz. The comparison was performed for six local weak-to-moderate magnitude events, spanning various azimuths, hypocenter depths, and distances. The earthquakes were recorded by the local array of surface and borehole accelerometers (see Fig. 2 and Table 5). Importantly for the numerical simulations, the hypocenters are located inside the 3D numerical box (as displayed in Fig. 2): the maximum size of this box was limited to roughly 20×30 km^2 to keep a reasonable computational time while going up to 4 Hz. This limited size excluded a number of more distant events with good signal-to-noise ratios, which will be included in a later study considering the improving capabilities of high-performance computers. Further requirements on the selected events were (1) available focal mechanism and (2) a sufficient number of high-quality recordings by the local seismic array. The synthetics to be compared with the records are computed for the 3D viscoelastic layered model A of the Mygdonian basin (Table 2).

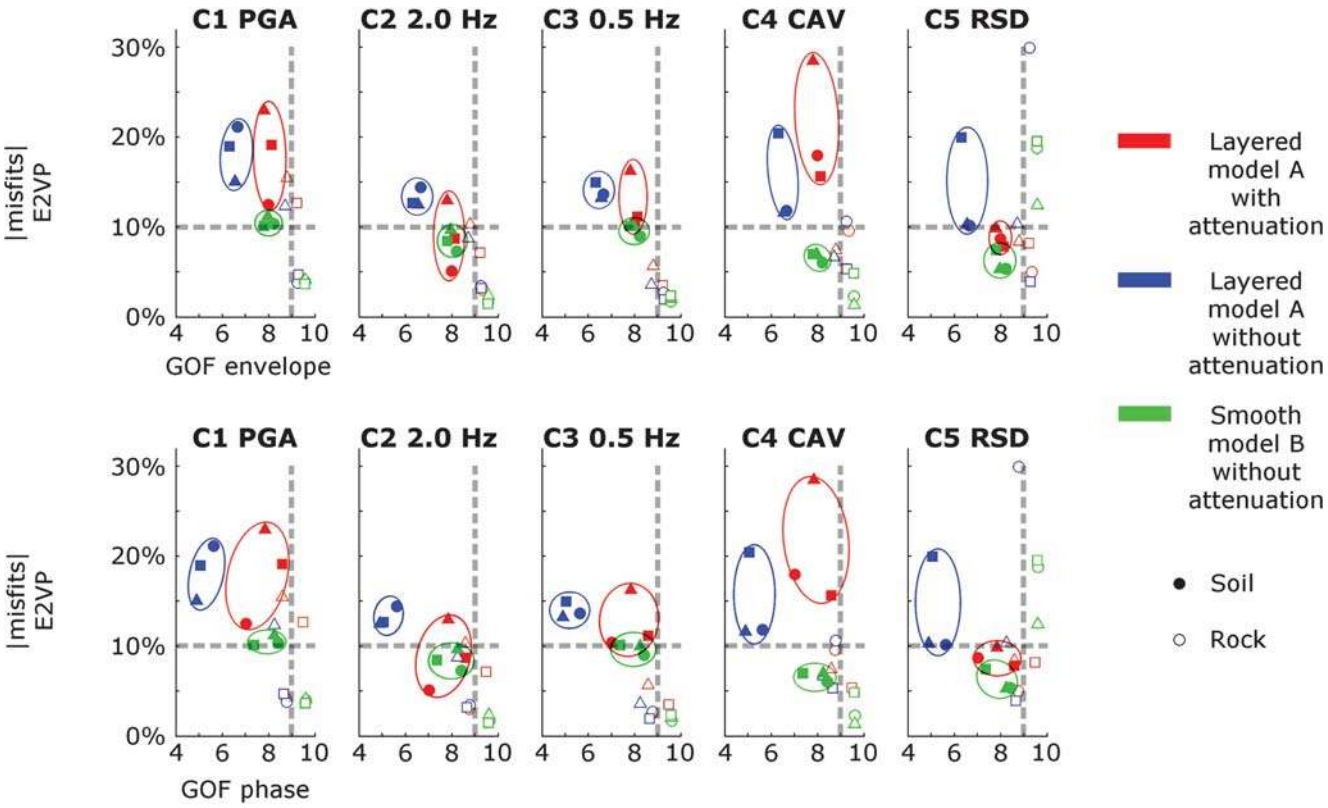

Figure 8. Comparison of GOF values (following the GOF procedure by Kristeková *et al.*, 2009) and horizontal absolute misfits obtained on the E2VP evaluation criteria C1–C5 (see the Appendix), for the three verification cases presented in this article and differentiated here by colors. The GOF values are computed as the weighted average over horizontal components of ground velocity in the envelope (top panels) and in phase (bottom panels) for team 3D01 relative to team 3D02 (circles), team 3D04 (triangles) and teams 3D11/3D09 (squares), depending on their availabilities. All values are weighted averages (weighting individual values by the corresponding time–frequency amplitude or target parameter, for GOF and C1–C5, respectively, to emphasize the misfits for the most important points), computed either on 19 rock sites (open symbols) or on 268 soil sites (solid symbols surrounded by an oval for each verification case).

Comparing Recordings and their Numerical Predictions for Event Number 4

The acceleration time histories recorded from the closest and largest event (number 4 in Fig. 2 and Table 5) are compared with the numerical predictions computed by three different teams at three receivers: the TST surface site at the center of the basin (soft soil, Fig. 9a), the TST 197 m deep borehole receiver (rock condition, Fig. 9b), and the surface site W03 located westward (soft soil, Fig. 9c). The numerical predictions look visually very similar to one another at each of these three sites. The highest level of agreement between recordings and numerical predictions is found on the north component of the surface and borehole receivers at the TST site, except for a slight time shift that is probably due to inaccuracy in the hypocenter location. These cases (i.e., event 4 and the TST site) are surely the best results of the whole validation exercise. At the opposite extreme, large discrepancies between recordings and numerical predictions appear in the waveforms at the W03 site, even if the maximum level of amplitude is

Table 5

Characteristics of Six Selected Real Events that Occurred near the Mygdonian Basin, for which the Recordings by the EUROSEISTEST Accelerometric Array are Compared to 3D Numerical Predictions

Event Number	Date (yyyy/mm/dd) (hh:mm:ss)	Magnitude M_w	Depth (km)	Hypocentral Distance at Central Site TST (km)	Strike (°)	Dip (°)	Rake (°)
2	2004/11/19 21:01:04	2.8	6.9	17.2	100	60	−50
4	2005/09/12 19:08:30	4.4	5.0	8.2	53	43	−127
5	2005/09/20 17:41:20	3.1	6.0	9.2	72	55	−113
6	2005/10/09 07:12:05	3.9	6.0	9.3	61	55	−115
7	2005/10/09 12:30:22	3.4	5.0	9.7	72	55	−113
8	2006/08/17 04:27:31	3.8	10.0	17.2	329	34	−64

See locations of epicenters in Figure 2. Event 8 was not recorded at central site TST.

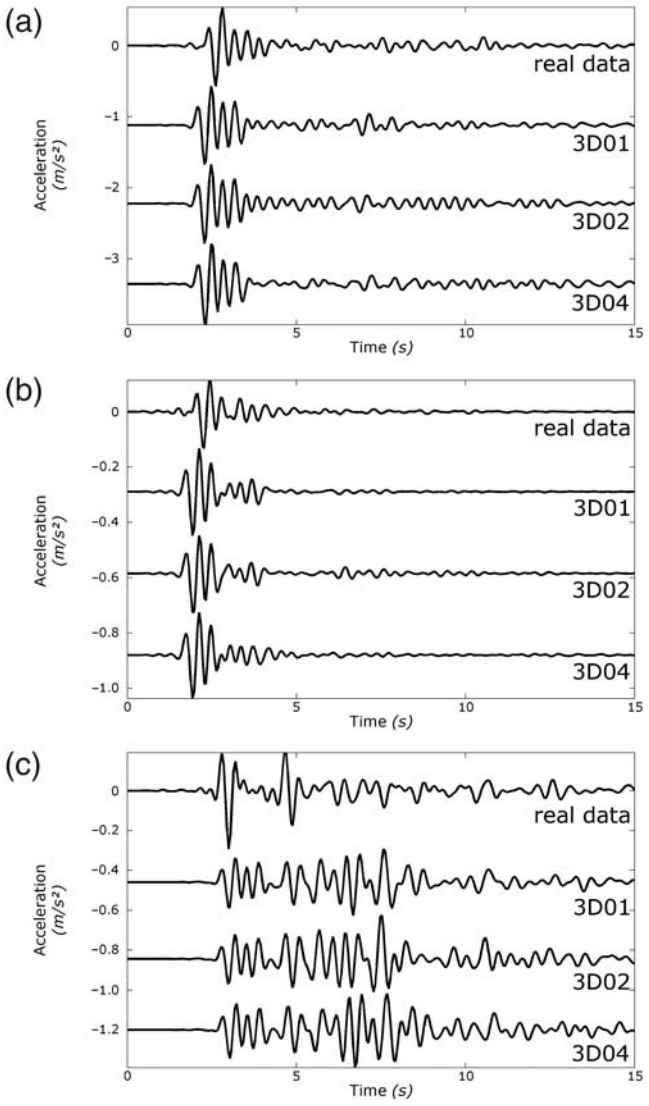

Figure 9. North–south component of observed and numerically predicted ground acceleration at (a) the central soil site TST at surface, (b) the corresponding 197 m depth borehole station, and (c) the west soil site W03, for the M_w 4.4 real event in the northeast (event 4 in Fig. 2 and Table 5). Every time series is Butterworth filtered between 0.5 and 4.0 Hz.

relatively well predicted and if the same event is considered.

To have a global view of the agreement between recordings of the event 4 and their numerical predictions for all recording sites, the horizontal components are compared in terms of misfits on the E2VP criteria C1–C5 (Fig. 10). The positive and negative misfit values, respectively, mean over- and underestimation of 3D01's prediction with respect to the recordings. The misfit values are highly variable on the whole array: an almost perfect fit (~0%) is achieved on a few receivers, but some high misfits (greater than ±100%) are also observed. The misfit values are also highly variable from one criterion to another. The visual comparison of recordings with their numerical predictions (Fig. 9) indicates a good level of agreement at the surface soil site TST (central receiver in Fig. 10) and at the corresponding downhole sensor at 197 m depth (the vertical array of five receivers below TST is represented in Fig. 10 by a diagonal projection of points at the surface). The level of agreement at the surface soil site TST is indeed excellent (misfits closed to 0%) for criteria C1, C2, and C4 (intermediate-to-high frequencies and CAV intensity). The misfit value for C3 remains reasonable (below 20%). As for C5, it was previously shown (see the Discussion on the Comparison Criteria section) that the duration criterion can lead to relatively strong misfits if the duration of the seismic signal is short; it is precisely the case at TST for close-event 4. The misfits shown in Figure 10 for the borehole station also drop to a satisfactory level (absolute values for all criteria are below 30%). On the contrary, the recorded waveform and the numerical predictions at the western site of the array are really different (Fig. 9c). It is noteworthy that, even if the waveforms are different, the numerical prediction is still able to reproduce some of the characteristics of the ground motion: the fit at the western site is excellent for C3 (low frequencies) and good for C4 (CAV intensity).

The highest misfits observed in Figure 10 are easily explainable. The amplitude of the ground motion at the eastern soil site (far-right colored dot) is systematically overestimated by the numerical prediction regardless of the frequency band considered (criteria C1–C4). That receiver is the closest receiver to the seismic source, and the numerical prediction is thus especially impacted by even small uncertainties in source characteristics (for instance, a slight error in the hypocenter location). At the northern rock site, the numerical prediction considerably underestimates amplitude of the recorded waveform (regardless of frequency range; C1–C3) and intensity (C4). The location of the station PRO, relative to the epicenter of event 4, is close to the azimuth of the nodal planes of the focal mechanism (see Fig. 2). Rapid spatial variations of amplitude and intensity of the ground motion are expected for such short distances from this azimuth: therefore, the numerical prediction at PRO for event 4 is highly sensitive to weak uncertainties in the focal mechanism. The overprediction of duration at this site is fully consistent with the underestimation of the amplitude of the main signal, resulting in a Husid plot spread over a larger time.

Comparing Verification and Validation Misfits for All Six Events

Those misfit values show that the validation results are very variable, even inside one event. A global overview of the validation exercise allows comparing the level of agreement between recordings and their numerical predictions to the agreement reached among different synthetics. Figure 11a gathers misfit values based on the E2VP criteria for the verification exercise (misfits between synthetics obtained by different teams; blue-tone dots) and for the validation exercise (misfits between recordings and numerical predictions; red-tone dots) at all receivers for the six selected events (Fig. 2

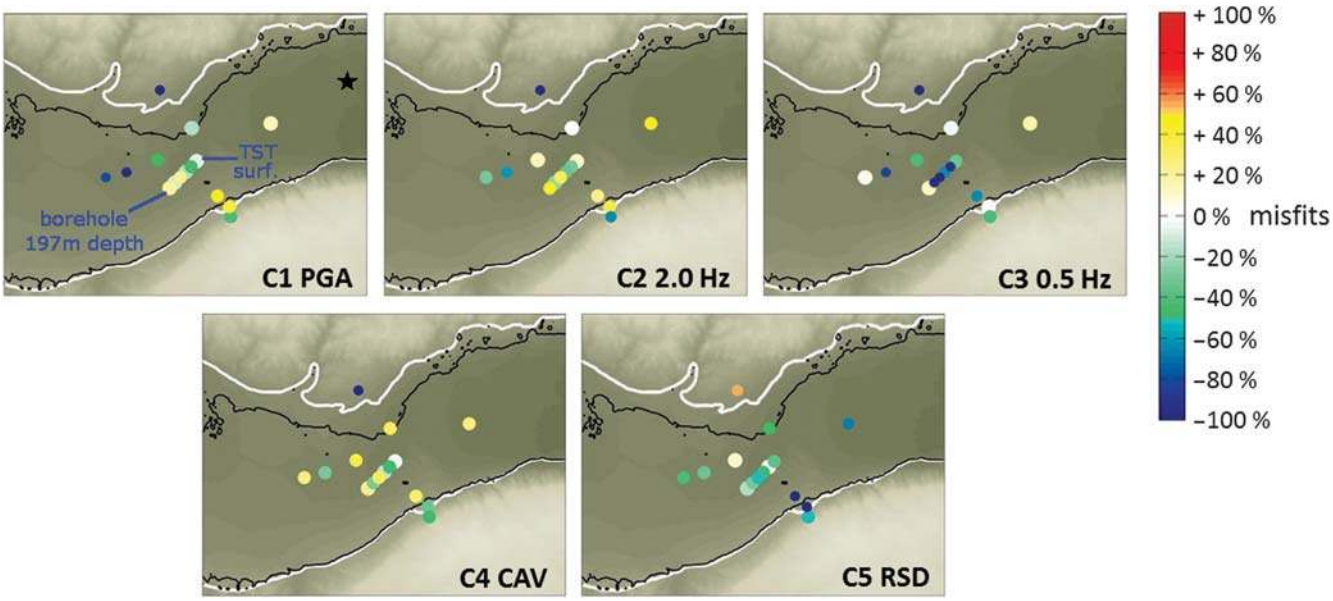

Figure 10. Maps of horizontal misfits on the E2VP evaluation criteria (see the How to Objectively Quantify the Similarity between Two Signals? section) between the recordings of real event 4 (black star; see also Fig. 2 and Table 5) and its numerical 3D prediction by team 3D01. C1 is based upon peak ground acceleration (PGA), C2 upon elastic spectral acceleration ranging between 1.5 and 3.0 Hz, C3 upon elastic spectral acceleration ranging between 0.375 and 0.750 Hz, C4 upon cumulative absolute velocity (CAV), and C5 upon 5%–95% relative significant duration. Each colored dot corresponds to the misfit obtained at the corresponding real receiver, the vertical array at TST being projected on the surface at the center of the map. Red/yellow tones are for overestimation of the numerical prediction compared to the recordings; blue/green tones are for underestimation.

and Table 5). The averaging over all receivers was obtained by (1) considering only absolute misfit values (L1 norm), so as to not balance overprediction at some sites by underprediction at others and (2) weighting the misfit value at each receiver by the value of the corresponding parameter, so as to emphasize the misfits for the most important points. An overall misfit around 25% is observed for the verification, whereas the misfit values are much higher for the validation (around 80%).

Figure 11b provides a complementary comparison by considering only one surface soil site (TST) for five events (one of the six events was not recorded at TST). The verification misfits remain approximately at the same level (around 25%), whereas the validation misfits are reduced to approximately 60%. Finally, Figure 11c focuses on the average misfit for the biggest event (event 4) at all receivers. A reduction of the misfit values to about 10% is observed for the verification and to about 40% for the validation. This synthesis, shown in Figure 11, clearly demonstrates the robustness of the statement that the smallest differences between recordings and their numerical predictions are significantly larger than the usual distances between simulations.

Discussion: Can We Identify the Origins of the Validation Misfits?

The details of the waveforms are highly sensitive to the source parameters (hypocenter location and focal mechanism), to the shape of the sediment-basement interface, and to the internal sediment layering of the basin. Each of these items may affect the validation misfits. Are the misfits due predominantly to inaccuracies in the description of the sources and/or of the 3D model? Figure 12 shows maps of the misfit values for criterion C4 (CAV) between actual recordings and their numerical prediction by team 3D02 for the six selected events in Figure 2 and Table 5. A first assumption consists of assigning the origin of mismatch between recordings and their numerical predictions to the uncertainties in source parameters. One could then expect that the higher the magnitude, the lower the misfits because larger-magnitude earthquakes are usually better characterized than low-magnitude earthquakes (for events moderate enough to assume a point source). Figure 12 shows that the best validation agreement is indeed obtained for the largest-magnitude event (event 4, M_w 4.4). Nevertheless, the second largest magnitude (event 6, M_w 3.9) produces the worst validation results, whereas the two lowest-magnitude events (event 2, M_w 2.8; event 5, M_w 3.1) produce the second best results. Within our dataset (limited to few events), no clear relation appears between the validation misfits and the magnitude or the hypocentral distance of those earthquakes.

Another hypothesis is to relate the origin of misfits to the uncertainties in the 3D distribution of the model properties. Depending on the level of knowledge in the model, some stations should systematically produce low misfits and good validation results (where the model properties are accurately defined), while other stations should systematically produce strong misfits (where the model properties are poorly defined), provided that the local response is predominantly

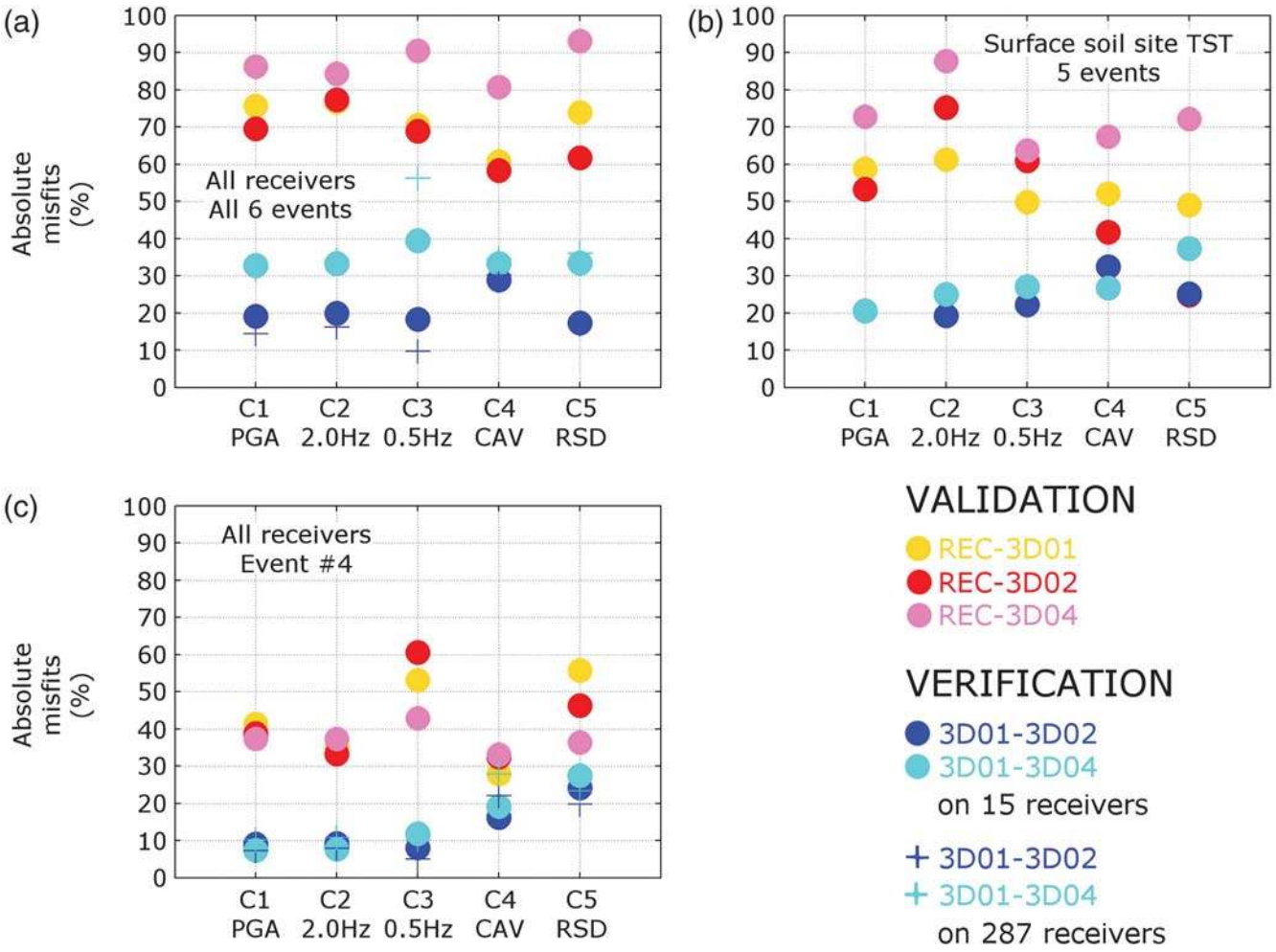

Figure 11. Summary of horizontal absolute misfits obtained on the E2VP evaluation criteria C1–C5 for the verification and validation exercises, considering different configurations: (a) average for the six selected events (Fig. 2 and Table 5) at all receivers; (b) average for the five events recorded at the central soil site TST; (c) average for the biggest event (event 4) at all receivers. Synthetics-to-synthetics misfits (verification, blue-tone dots) are compared to recordings-to-synthetics misfits (validation, warm-tone dots). The verification misfits in the left panels are computed by taking into account either the real array (limited to 15 surface receivers; solid circles) or the complete virtual array (287 receivers; crosses). A single value per array is obtained by calculating the weighted average of the absolute misfits over the considered receivers, weighting each individual misfit by the corresponding target value of the ground-motion parameter (to decrease the importance of weaker points).

controlled by the local structure. Nothing similar can be observed in Figure 12.

To remove (some of) the errors due to uncertainties in source parameters and to focus on the prediction of the site effect alone, Figure 13 evaluates the prediction of the Fourier transfer function from the downhole sensor to the surface sensor at the central vertical array TST. The instrumental site-to-reference spectral ratio derived from the actual recordings of event 4 (gray line) is compared to those derived from 3D synthetics (back lines). The frequencies at which amplification of ground motion occurs (around 0.75 Hz for the fundamental peak, 1.7 and 2.8 Hz for overtones, and around 1.0 Hz probably due to the excitation of local surface waves) are well reproduced in all synthetics. However, the amplitudes of these different maxima are not all accurately predicted. The overtone at 2.8 Hz and the contribution of the surface waves at 1 Hz are significantly underestimated. We estimate that the numerical predictions have well reproduced some features of the site effect, but not all.

Respective Influence of the Uncertainties in Source and Model

To deepen the analysis of the actual capability to numerically predict the site-effect component, synthetic time histories that could both maximize the impact of the numerical estimate of the site-effect component and minimize the effect of uncertainties in the source description are required. Toward that goal, we compute hybrid time histories: the complex synthetic spectral ratio between the surface and downhole TST sensors, as derived from the numerical computation (i.e., with both modulus and phase), is considered as the borehole–surface transfer function and is thus multiplied

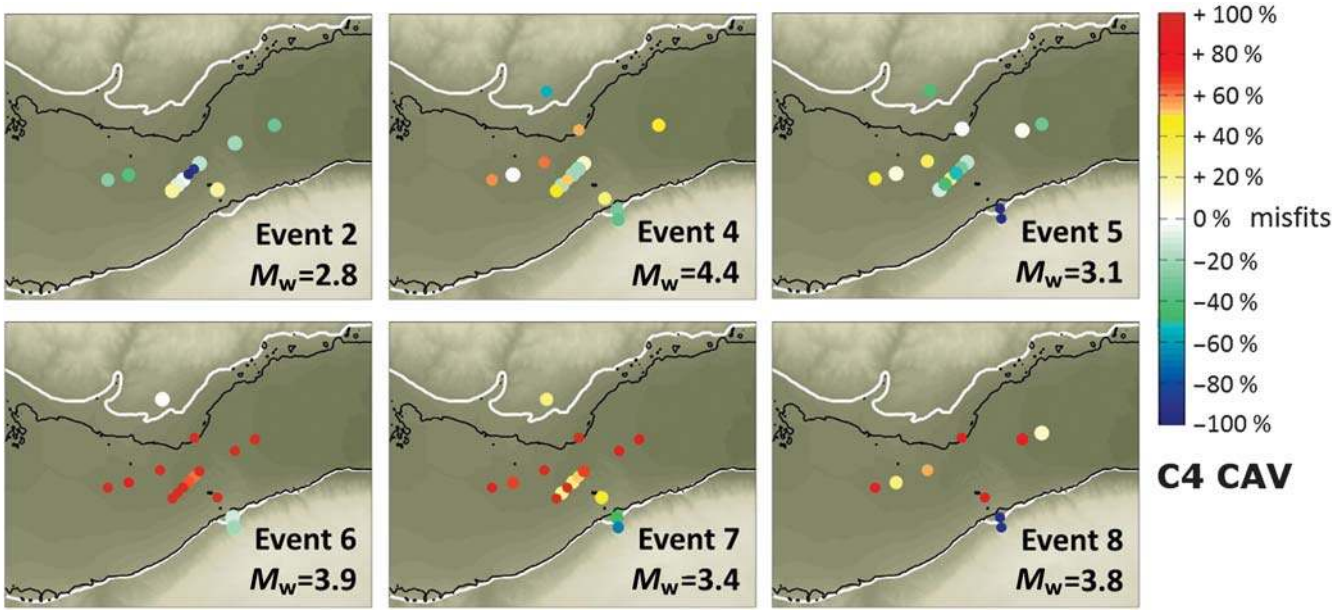

Figure 12. Locations of horizontal misfits for criterion C4 (CAV) between the real recordings of the six selected events (see Fig. 2 and Table 5) and their numerical 3D predictions by team 3D02. Each colored dot corresponds to the misfit obtained at the corresponding real receiver, the vertical array at TST being projected onto the surface at the center of the map. Red tones are for overestimation of the numerical prediction compared to the recordings, blue tones are for underestimation.

in the Fourier domain, with the actual signal recorded at the downhole sensor. The inverse Fourier transform returns a hybrid time history in the sense that the input signal is a real signal (integrating actual source parameters), whereas the site-effect part is coming from the numerical predictions. This way the effect of uncertainties in the source description is somehow removed (we consider the sensitivity of the transfer function to uncertainties in source parameters is very weak as long as the precision on hypocenter location remains within a few kilometers; Chaljub *et al.*, 2014). The E2VP evaluation criteria are then applied between the actual recordings and the hybrid time histories computed at the surface soil site TST for five of the selected events (event 8 was not recorded at TST) using the actual recordings at the downhole rock site and the numerical transfer function predicted by three teams (3D01, 3D02, and 3D04). Figure 14 displays the misfits obtained following this procedure and their comparison to the previous validation misfits obtained between actual recordings and their fully numerical predictions. Figure 14a demonstrates that for all C1–C5 criteria, the absolute misfit values obtained with hybrid signals are significantly lower than the values obtained with fully numerical signals (around 35% instead of 60%). Because hybrid signals may be considered as free from effects of source uncertainties, one may conclude that the origins of discrepancies between actual recordings and their numerical predictions are likely to be almost equally balanced between uncertainties in source parameters and uncertainties in the 3D model description.

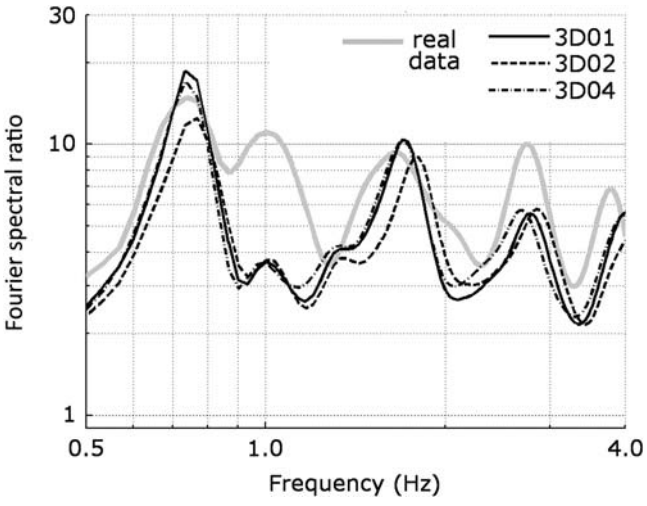

Figure 13. Fourier spectral ratios at the central site TST, computed between the surface receiver and the borehole receiver at 197 m depth for the average horizontal component recorded or numerically predicted for the M_w 4.4 event in the northeast (event 4 in Fig. 2 and Table 5). The results are shown for three different numerical predictions (black lines), to be compared to the real data (gray bold line). The spectral ratios from this event are representative of the median spectral ratios computed for the five selected events recorded at TST.

Figure 14b presents the same results with average computed over signed misfit values (the ± sign of the misfit value respectively indicating over- or underestimation of the target is kept; see the Appendix) and allows the process to be extended one step further: fully numerical predictions exhibit a trend to overestimate most parameters (C1–C4), whereas the hybrid predictions exhibit an opposite trend to underestimate the same parameters, in perfect agreement with the surface/downhole spectral ratios displayed in Figure 13. This suggests that: (1) In the present case, uncertainties in source description

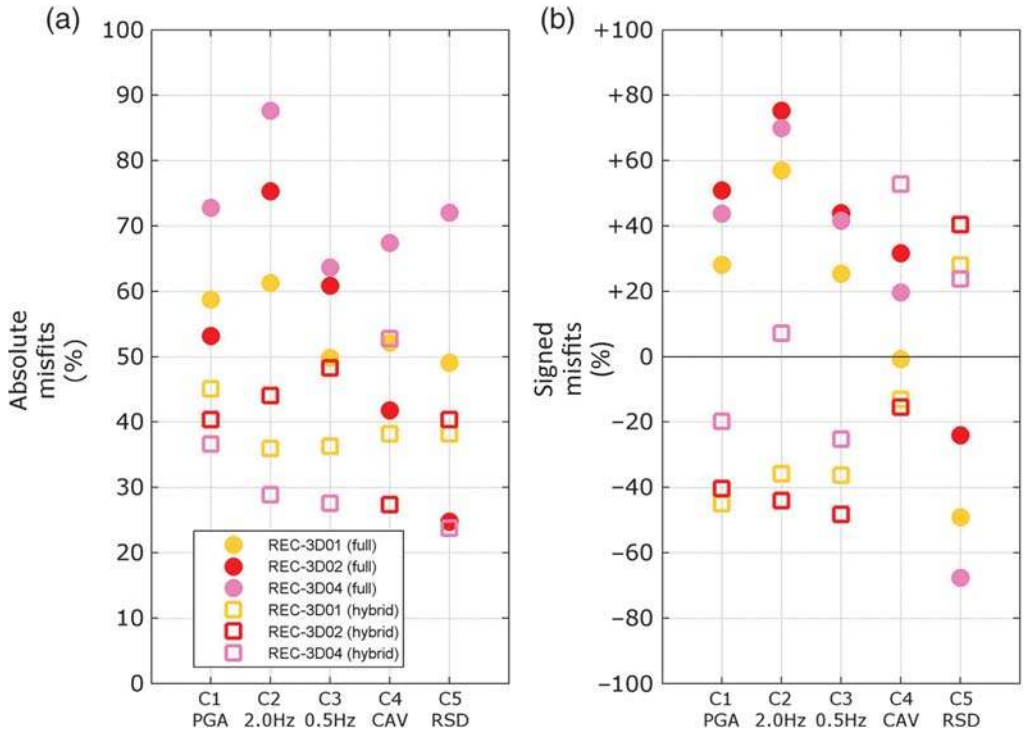

Figure 14. Average of (a) absolute misfit values and (b) signed misfit values obtained on the E2VP evaluation criteria C1–C5 for the five events recorded and numerically predicted by teams 3D01, 3D02, and 3D04 at the central soil site TST. The actual recordings are compared to fully numerical predictions (full circles) and to hybrid predictions (see the Respective Influence of the Uncertainties in Source and Model section; empty squares).

tend to produce overestimation of the ground motion in the E2VP validation exercise (that could be explained by an overestimation of the magnitude; for example, the signals used for magnitude estimation could be insufficiently corrected for site effects). (2) The site effect itself is globally underestimated at the TST site. That global trend for underestimating the actual amplification by all the 3D simulations at the TST site (it could not be investigated at other sites, as there is no other downhole sensor) could have several explanations: incorrect estimates of damping (too large values), incorrect internal sediment layering structure, overemphasis on the buried-pass or saddle-point structure just underneath the TST site (which would result in larger off-profile diffraction), or overestimation of the hypocentral depth, resulting in too-weak excitation of surface waves.

Conclusions

The participation of several computational teams from various parts of the world, with expertise in advanced numerical codes, allowed achievement of several major accomplishments in the verification and validation of 3D ground-motion simulation codes. A very good similarity, quantified with an objective scale, could be obtained among synthetics up to a frequency of 4 Hz despite the relative complexity of 3D models, which witnesses the accuracy of the corresponding numerical schemes. The existence of an excellent agreement between several completely independent codes, with code-to-code differences much smaller than predictions-to-observations differences, makes it possible and legitimate to include the numerical simulation approach in the toolbox for site-specific ground-motion estimation, at least in the 3D linear case and low-to-intermediate frequency range.

A careful verification exercise requires time, whereas a careful validation exercise also requires high-quality data. The most common outcome of the verification phase (similarly to the conclusions of Chaljub *et al.*, 2010) is that, without iterations and cross checking, different codes are very likely to provide significantly different results when applied to the same case study. As an immediate conclusion, too fast applications of 3D codes may yield wrong ground-motion estimates, potentially resulting in increased mistrust in end users. The lessons and experiences of E2VP draw attention to the following recommendations for a wise and careful use of such numerical simulation codes.

One should never be satisfied with only one computation from one single team, but should request several teams (at least two) with different numerical schemes to perform parallel computations of the same case. The corresponding results then can be considered reliable only if they agree beyond some quantitative threshold; a GOF threshold of 7 seems a reasonable value and roughly corresponds to misfit thresholds for the C1–C5 criteria within about 20%–25%.

Comparison of numerical predictions with actual data (*in situ* earthquake recordings) is always useful. Having sensitive *in situ* instrumentation (continuously recording broadband

velocimeters or accelerometers) proves to be invaluable for checking the reliability of numerical simulation results, with a special emphasis on vertical arrays, which allow the site-effect component to be constrained. In addition to the availability of high-quality *in situ* recordings, the validation phase showed the importance of completing such data with high-quality metadata, concerning both the source parameters and the site model. Even though the need for additional information and complementary surveys can always be identified, the site selected for the present project can be considered as one of the best-known sites, at least in the Euro-Mediterranean area. The results obtained here in terms of validation, and comparison with actual recordings should thus be representative of the top-ranking sites in terms of site investigations.

Even in such a well-known site, the prediction of several ground-motion parameters of engineering interest exhibits average differences around 60%–80%, with a minimum of 30%–40% for the larger magnitude, probably best-known event. Such values should be kept in mind when discussing the effects of missing elements in the numerical approach (e.g., nonlinearities). The gross characteristics of the amplification at the valley center are satisfactorily reproduced by the 3D model, both in terms of spectral contents and signal duration, although with a slight underestimation. In the present case, the differences between recordings and numerical predictions appear to have an approximately balanced origin shared between inaccuracies in source parameters (hypocenter location, magnitude, and focal mechanism), and uncertainties in the site model (geometry, velocity structure, and damping). Interestingly, in the present case, the former are associated with some overprediction of ground motion, whereas the latter would underestimate the site amplification. Such observations suggest a positive bias in magnitude estimates, which would be consistent with an underestimation of site effects at most observational stations. However, similar analyses on other sites are required to indicate whether such observations can be generalized or are specific to the considered site.

Two final comments concerning the validation phase are worth consideration. The first is related to the small number of candidate seismic events that could be considered (i.e., those within the numerical box). This is indeed a typical situation for moderate/weak seismicity areas. Future validation exercises would certainly benefit from the possibility of including more distant events, which implies either the increase of computing capabilities or the use of hybrid numerical schemes coupling computations at different scales (an excitation box).

The second comment deals with the consequences of these results on the use of numerical simulation for ground-motion prediction. In the case of a deterministic approach, a scenario earthquake would be defined: all the uncertainties affecting the validation and linked to source parameters (partially responsible for the large differences between recordings and their numerical predictions) should therefore be left aside, and only those linked to the propagation and site models should be considered; however, for sources of finite extent, an additional cause of variability should be taken into account as the detailed rupture kinematics cannot be deterministically predicted, but it should be tackled with some sensitivity study. In the case of a probabilistic approach, the use of numerical simulation would probably focus more on the determination of the site amplification function than on massive simulations with a wide range of source parameters (location and magnitude). Therefore, whatever the approach, the main focus is the determination of the site amplification. Further investigations of the validation of 3D numerical simulations should thus definitely favor the use of pairs of stations on the site of interest and on relevant nearby reference, including local vertical arrays, together with thorough geophysical and geotechnical surveys to provide the required details of the underground structure, not only for high frequencies and short wavelengths, but also for some still badly known parameters, such as material damping.

Data and Resources

Several numerical cases of the E2VP are made freely available to the seismological community at http://www.sismowine.org (last accessed February 2015). The real seismograms used in this study can be obtained from the EUROSEISTEST strong ground-motion database and web portal at http://euroseisdb.civil.auth.gr (last accessed June 2014; see also Pitilakis *et al.*, 2013). The spectral-element method (SEM) meshes were designed using the commercial software Cubit (https://cubit.sandia.gov; last accessed June 2014). The synthetic seismograms from team 3D11 were computed using the code EFISPEC3D (De Martin, 2011; http://efispec.free.fr; last accessed January 2014).

Acknowledgments

The authors thank all the participants of the EUROSEISTEST Verification and Validation Project and acknowledge the Cashima project (funded by Commissariat à l'énergie atomique et aux énergies alternatives [CEA] and Laue-Langevin Institute [ILL]) for its financial support. We thank Robert W. Graves and an anonymous reviewer for their careful review of this work.

The simulations of team 3D01 were performed in the Computing Centre of the Slovak Academy of Sciences using the supercomputing infrastructure acquired in project ITMS 26230120002 and 26210120002 (Slovak infrastructure for high-performance computing) supported by the Research and Development Operational Program funded by the European Regional Development Fund (ERDF). The simulations of team 3D02 were performed on the CIMENT infrastructure, Grenoble, France. The simulations of team 3D04 were performed on the computational resources of Consorzio Interuniversitario per il Calcolo Automatico (CINECA), Bologna, Italy. The simulations of team 3D09 were performed on the high-performance computing facilities of Institut du Développement et des Ressources en Informatique Scientifique (IDRIS)/Centre National de la Recherche Scientifique (CNRS) and of the Observatoire de la Côte d'Azur (OCA), France. This research was also partly funded by Bureau des Recherches Géologiques et Minières (BRGM) internal funds for project SEISMORISK.

References

Anderson, J. G. (2004). Quantitative measure of the goodness-of-fit of synthetic seismograms, *13th World Conf. on Earthquake Engineering Conf. Proc.*, Vancouver, British Columbia, Canada, 1–6 August, Paper Number 243.

Bard, P.-Y. (1992). Discussion session: Lessons, issues, needs and prospects, special theme session 5: Turkey Flat and Ashigara Valley experiments, *10th World Conf. on Earthquake Engineering Conf. Proc.*, Madrid, Spain, 19–24 July, 6985–6988.

Bielak, J., R. W. Graves, K. B. Olsen, R. Taborda, L. Ramírez-Guzmán, S. M. Day, G. P. Ely, D. Roten, T. H. Jordan, P. J. Maechling, *et al.* (2010). The ShakeOut earthquake scenario: Verification of three simulation sets, *Geophys. J. Int.* **180,** 375–404, doi: 10.1111/j.1365-246X.2009.04417.x.

Campbell, K. W., and Y. Bozorgnia (2010). A ground motion prediction equation for the horizontal component of cumulative absolute velocity (CAV) based on the PEER-NGA strong motion database, *Earthq. Spectra* **26,** no. 3, 635–650, doi: 10.1193/1.3457158.

Chaljub, E., C. Cornou, and P.-Y. Bard (2006). Numerical benchmark of 3D ground motion simulation in the valley of Grenoble, French Alps, *Third International Symposium on the Effects of Surface Geology on Seismic Motion*, Grenoble, France, 30 August–1 September, Paper Number SB1, Vol. 2.

Chaljub, E., D. Komatitsch, J.-P. Vilotte, Y. Capdeville, B. Valette, and G. Festa (2007). Spectral element analysis in seismology, in *Advances in Wave Propagation in Heterogeneous Media*, R.-S. Wu and V. Maupin (Editors), in Advances in Geophysics, R. Dmowska (Series Editor), Academic Press London, United Kingdom, Vol. 48, 365–419.

Chaljub, E., E. Maufroy, F. De Martin, F. Hollender, C. Guyonnet-Benaize, M. Manakou, A. Savvaidis, A. Kiratzi, Z. Roumelioti, and N. Theodoulidis (2014). How sensitive is earthquake ground motion to source parameters? Insights from a numerical study in the Mygdonian basin, EGU General Assembly, *Geophys. Res. Abstr.* **16,** EGU2014–11738.

Chaljub, E., E. Maufroy, P. Moczo, J. Kristek, F. Hollender, P.-Y. Bard, E. Priolo, P. Klin, F. De Martin, Z. Zhang, *et al.* (2015). 3-D numerical simulations of earthquake ground motion in sedimentary basins: Testing accuracy through stringent models, *Geophys. J. Int.* **201,** no. 1, 90–111, doi: 10.1093/gji/ggu472.

Chaljub, E., P. Moczo, S. Tsuno, P.-Y. Bard, J. Kristek, M. Käser, M. Stupazzini, and M. Kristeková (2010). Quantitative comparison of four numerical predictions of 3D ground motion in the Grenoble valley, France, *Bull. Seismol. Soc. Am.* **100,** no. 4, 1427–1455.

Clayton, R., and B. Engquist (1977). Absorbing boundary conditions for acoustic and elastic wave equations, *Bull. Seismol. Soc. Am.* **67,** no. 6, 1529–1540.

Cramer, C. H. (1995). Weak-motion observations and modeling for the Turkey Flat, U.S., site-effects test area near Parkfield, California, *Bull. Seismol. Soc. Am.* **85,** no. 2, 440–451.

Day, S. M., J. Bielak, D. Dreger, R. Graves, S. Larsen, K. B. Olsen, and A. Pitarka (2001). Tests of 3D elastodynamic codes: Final report for Lifelines project 1a01, *Technical Report*, Pacific Earthquake Engineering Research Center and Southern California Earthquake Center.

Day, S. M., J. Bielak, D. Dreger, R. Graves, S. Larsen, K. B. Olsen, and A. Pitarka (2003). Tests of 3D elastodynamic codes: Final report for Lifelines project 1a02, *Technical Report*, Pacific Earthquake Engineering Research Center.

Day, S. M., J. Bielak, D. Dreger, R. Graves, S. Larsen, K. B. Olsen, and A. Pitarka (2005). 3D ground motion simulations in basins: Final report for lifelines project 1a03, *Technical Report*, Pacific Earthquake Engineering Research Center.

De Martin, F. (2011). Verification of a spectral-element method code for the Southern California Earthquake Center LOH.3 viscoelastic case, *Bull. Seismol. Soc. Am.* **101,** no. 6, 2855–2865.

Electrical Power Research Institute (EPRI) (1988). A criterion for determining exceedance of the operating basis earthquake, *Report No. EPRI NP-5930*, Palo Alto, California.

Etienne, V., E. Chaljub, J. Virieux, and N. Glinsky (2010). An *hp*-adaptive discontinuous Galerkin finite-element method for 3-D elastic wave modeling, *Geophys. J. Int.* **183,** no. 2, 941–962, doi: 10.1111/j.1365-246X.2010.04764.x.

Graves, R. W. (1996). Simulating seismic wave propagation in 3D elastic media using staggered-grid finite differences, *Bull. Seismol. Soc. Am.* **86,** no. 4, 1091–1106.

Jongmans, D., K. Pitilakis, D. Demanet, D. Raptakis, J. Riepl, C. Horrent, K. Lontzetidis, and P.-Y. Bard (1998). EURO-SEISTEST: Determination of the geological structure of the Volvi basin and validation of the basin response, *Bull. Seismol. Soc. Am.* **88,** no. 2, 473–487.

Kawase, H., and T. Iwata (1998). A report on submitted results of the simultaneous simulation for Kobe, in *The Effects of Surface Geology on Seismic Motion, Recent Progress and New Horizon on ESG Study*, Vol. 3, Balkema/CRC Press, Leiden, The Netherlands.

Kawase, H., and S. Matsushima (1998). Strong motion simulation in Kobe during the Hyogo-ken Nanbu earthquake of 1995 based on a three-dimensional basin structure, *J. Struct. Constr. Eng. Trans. Architec. Inst.* **514,** 111–118.

Kempton, J. J., and J. P. Stewart (2006). Prediction equations for significant duration of earthquake ground motions considering site and near-source effects, *Earthq. Spectra* **22,** no. 4, 985–1013, doi: 10.1193/1.2358175.

Klin, P., E. Priolo, and G. Seriani (2010). Numerical simulation of seismic wave propagation in realistic 3-D geo-models with a Fourier pseudo-spectral method, *Geophys. J. Int.* **183,** no. 2, 905–922, doi: 10.1111/j.1365-246X.2010.04763.x.

Komatitsch, D., Q. Liu, J. Tromp, P. Süss, C. Stidham, and J. H. Shaw (2004). Simulations of ground motion in the Los Angeles basin based upon the spectral-element method, *Bull. Seismol. Soc. Am.* **94,** 187–206, doi: 10.1785/0120030077.

Kristek, J., P. Moczo, and R. J. Archuleta (2002). Efficient methods to simulate planar free surface in the 3D 4th-order staggered-grid finite-difference schemes, *Stud. Geophys. Geod.* **46,** no. 2, 355–381.

Kristek, J., P. Moczo, and M. Gális (2010). Stable discontinuous staggered grid in the finite-difference modeling of seismic motion, *Geophys. J. Int.* **183,** no. 3, 1401–1407, doi: 10.1111/j.1365-246X.2010.04775.x.

Kristeková, M., J. Kristek, and P. Moczo (2009). Time-frequency misfit and goodness-of-fit criteria for quantitative comparison of time signals, *Geophys. J. Int.* **178,** 813–825, doi: 10.1111/j.1365-246X.2009.04177.x.

Kristeková, M., J. Kristek, P. Moczo, and S. M. Day (2006). Misfit criteria for quantitative comparison of seismograms, *Bull. Seismol. Soc. Am.* **96,** no. 5, 1836–1850, doi: 10.1785/0120060012.

Manakou, M. (2007). Contribution to the determination of a 3D soil model for site response analysis, the case of the Mygdonian basin, *Ph.D. Thesis*, Department of Civil Engineering, Aristotle University of Thessaloniki, Greece.

Manakou, M., D. Raptakis, P. I. Apostolidis, F. J. Chávez-García, and K. Pitilakis (2007). The 3D geological structure of the Mygdonian sedimentary basin (Greece), *4th International Conference on Earthquake Geotechnical Engineering*, Thessaloniki, Greece, 25–28 June, Paper Number 1686.

Manakou, M., D. Raptakis, F. J. Chávez-García, P. I. Apostolidis, and K. Pitilakis (2010). 3D soil structure of the Mygdonian basin for site response analysis, *Soil Dynam. Earthq. Eng.* **30,** 1198–1211.

Martin, R., and D. Komatitsch (2009). An unsplit convolutional perfectly matched layer technique improved at grazing incidence for the viscoelastic wave equation, *Geophys. J. Int.* **179,** no. 1, 333–344, doi: 10.1111/j.1365-246X.2009.04278.x.

Moczo, P., J. Kristek, and M. Gális (2004). Simulation of the planar free surface with near-surface lateral discontinuities in the finite-difference modeling of seismic motion, *Bull. Seismol. Soc. Am.* **94,** no. 2, 760–768.

Moczo, P., J. Kristek, and M. Gális (2014). *The Finite-Difference Modelling of Earthquake Motions Waves and Ruptures*, Cambridge University Press, Cambridge, United Kingdom.

Moczo, P., J. Kristek, V. Vavryčuk, R. J. Archuleta, and L. Halada (2002). 3D heterogeneous staggered-grid finite-difference modeling of seismic motion with volume harmonic and arithmetic averaging of elastic moduli and densities, *Bull. Seismol. Soc. Am.* **92,** no. 8, 3042–3066.

Papazachos, C. B. (1998). Crustal *P*- and *S*-velocity structure of the Serbomacedonian Massif (northern Greece) obtained by non-linear inversion of traveltimes, *Geophys. J. Int.* **134,** 25–39, doi: 10.1046/j.1365-246x.1998.00558.x.

Peter, D., D. Komatitsch, Y. Luo, R. Martin, N. Le Goff, E. Casarotti, P. Le Loher, F. Magnoni, Q. Liu, C. Blitz, *et al.* (2011). Forward and adjoint simulations of seismic wave propagation on fully unstructured hexahedral meshes, *Geophys. J. Int.* **186,** no. 2, 721–739, doi: 10.1111/j.1365-246X.2011.05044.x.

Pitarka, A. (1999). 3D elastic finite-difference modeling of seismic motion using staggered grids with nonuniform spacing, *Bull. Seismol. Soc. Am.* **89,** no. 1, 54–68.

Pitilakis, K., G. Manos, D. Raptakis, A. Anastasiadis, K. Makra, and M. Manakou (2009). The EUROSEISTEST experimental test site in Greece, *EGU General Assembly*, Vienna, Austria, 19–24 April.

Pitilakis, K., Z. Roumelioti, D. Raptakis, M. Manakou, K. Liakakis, A. Anastasiadis, and D. Pitilakis (2013). The EUROSEISTEST strong ground motion database and web portal, *Seismol. Res. Lett.* **84,** no. 5, 796–804.

Raptakis, D., F. J. Chávez-García, K. Makra, and K. Pitilakis (2000). Site effects at Euroseistest-I: Determination of the valley structure and confrontation of observations with 1D analysis, *Soil Dynam. Earthq. Eng.* **19,** 1–22.

Raptakis, D., M. Manakou, F. J. Chávez-García, K. Makra, and K. Pitilakis (2005). 3D configuration of Mygdonian basin and preliminary estimate of its site response, *Soil Dynam. Earthq. Eng.* **25,** 871–887.

Satoh, T., H. Kawase, T. Sato, and A. Pitarka (2001). Three-dimensional finite-difference waveform modeling of strong motions observed in the Sendai basin, Japan, *Bull. Seismol. Soc. Am.* **91,** 812–825, doi: 10.1785/0120000086.

Stacey, R. (1988). Improved transparent boundary formulations for the elastic-wave equation, *Bull. Seismol. Soc. Am.* **78,** no. 6, 2089–2097.

Trifunac, M. D., and A. G. Brady (1975). On the correlation of seismic intensity scales with the peaks of recorded strong ground motion, *Bull. Seismol. Soc. Am.* **65,** no. 1, 139–162.

Tsuno, S., E. Chaljub, and P.-Y. Bard (2006). Grenoble valley simulation benchmark: Comparison of results and main learning, *Third International Symposium on the Effects of Surface Geology on Seismic Motion*, Grenoble, France, 30 August–1 September, Paper Number SB2, Vol. 2.

Appendix

The E2VP Ground-Motion Evaluation Criteria

To evaluate the extent of similarity between two mismatched signals within the EUROSEISTEST Verification and Validation Project (E2VP), we elaborated comparisons based on a series of complementary ground-motion parameters, each one emphasizing a different characteristic of the waveforms. To keep a reasonable number of parameters, the E2VP evaluation criteria are restricted to five parameters (three for amplitude/frequency content, one for energy, and one for duration) chosen as followed: (1) C1, peak ground acceleration (PGA); (2) C2, elastic spectral acceleration in intermediate frequencies, arithmetic average over 1.5–3.0 Hz; (3) C3, elastic spectral acceleration in low frequencies, arithmetic average over 0.375–0.750 Hz; (4) C4, cumulative absolute velocity (CAV); and (5) C5, relative significant duration (RSD) between 5% and 95% of the Arias intensity.

Criteria C1–C3 evaluate the amplitude of the signal in different frequency bands. These different frequency bands are chosen according to the observed characteristics of the real signals at the center of the Mygdonian basin: the frequency range evaluated by C3 includes the fundamental resonance frequency of the basin, whereas C2 covers the two higher modes.

Criterion C4 is based on the CAV, which is defined as the integral of the absolute value of the acceleration time series (Electrical Power Research Institute [EPRI], 1988):

$$\mathrm{CAV} = \int_0^{D_{\max}} |a(t)|dt, \tag{A1}$$

in which $|a(t)|$ is the absolute value of the acceleration time series at time t and $D_{\max}$ represents the total duration of the time series. Anderson (2004) proposed the Arias intensity and the energy integral as ground-motion parameters representative of the signal's intensity; both parameters are computed from the square of the acceleration or velocity time series. CAV is chosen as an alternative in the E2VP evaluation procedure because this parameter is of the same dimension as the three amplitude and frequency-content criteria C1, C2, and C3, therefore giving misfit values of the same order. CAV was found to be the instrumental intensity measure that best correlates with the onset of structural damage to engineered structures (EPRI, 1988; Campbell and Bozorgnia, 2010).

The duration criterion C5 is based on the RSD, which is defined as the time interval over which a specified amount of energy is dissipated. One common measure of the significant duration is the time interval between 5% and 95% of the Arias intensity I_A (Trifunac and Brady, 1975; Kempton and Stewart, 2006):

$$I_A = \left(\frac{\pi}{2g}\right) \int_0^{D_{\max}} a^2(t)dt, \tag{A2}$$

in which $a(t)$ is the acceleration time history, g is the acceleration of gravity, and $D_{\max}$ represents the total duration of the time series. The 5%–95% RSD is chosen in the E2VP evaluation procedure because it does not account for the timing of arrival of the different phases of energy. A slight time shift is frequently encountered when comparing recordings with their numerical predictions, possibly due to some mislocation of the source or to uncertainties in the bedrock velocity structure. That problem, easily identified by comparing arrival times at rock sites, does not affect the impact of ground motion on structures and is therefore of a secondary importance with respect to the E2VP purposes.

Prior to the computation of the misfits, the same processing is performed on both time series to be compared. They are cut to the same duration in time (generally to the shorter length of the numerical prediction, or 30 s in the present study). Both are band-pass filtered using a sixth-order Butterworth filter with corner frequencies of 0.05 Hz and of the maximum frequency available in the numerical prediction (4 Hz in the present study).

The comparison of two signals involves a prediction (a synthetic ground motion) being compared to the target, which is either the corresponding real recording or another prediction (eventually considered as a reference signal). The misfit δ_P between the target and its prediction for one ground-motion parameter P is therefore expressed in percentage of the target parameter P_{target} with the logarithm formulation

$$\delta_P = \left(\frac{(\log(P_{\text{pred.}}/P_{\text{target}})}{\log(2)} \right) \times 100. \qquad \text{(A3)}$$

This calculation of the misfit δ_P gives symmetrical values for under- or overestimation of the target value: δ_P is negative when the prediction underestimates the target and positive when the prediction overestimates the target.

In the E2VP evaluation procedure, the horizontal components of the ground motion are handled differently, depending on the considered ground-motion parameter. At first, each parameter is estimated over distinct horizontal components, giving two horizontal values per ground motion. Both C4 and C5 are based on the integral of the acceleration time series; therefore, the two horizontal values of the corresponding parameter (CAV and RSD) are directly added together prior to the comparison. Concerning C1–C3, the horizontal components of the target signal are systematically rotated, ranging from 0° to 355°, with an angle increment of 5°, to determine the rotation of components that maximizes the value of the considered parameter. This systematic exploration is performed on the acceleration time series for C1 and on the elastic spectral acceleration for C2 and C3. Once the maximizing rotation angle is determined, the same rotation is applied to the predictive signal. The comparison finally occurs on the horizontal component rotated to maximize the value of the target parameter.

University Grenoble Alpes
ISTerre, CNRS, IRD, IFSTTAR
BP 53, F-38041 Grenoble CEDEX 09
France
emeline.maufroy@ujf-grenoble.fr
emmanuel.chaljub@ujf-grenoble.fr
pierre-yves.bard@ujf-grenoble.fr
(E.M., E.C., P.-Y.B.)

CEA Cadarache
French Alternative Energies and Atomic Energy Commission
DPIE/SA2S/GAS
Bât. 352, F-13108 St. Paul Les Durance
France
fabrice.hollender@cea.fr
cedric.guyonnet-benaize@hotmail.fr
(F.H., C.G.-B.)

Comenius University Bratislava
Faculty of Mathematics, Physics and Informatics
Geophysical Institute
Slovak Academy of Sciences
Mlynská dolina F2
84248 Bratislava 4
Slovakia
kristek@fmph.uniba.sk
moczo@fmph.uniba.sk
(J.K., P.M.)

Istituto Nazionale di Oceanografia e di Geofisica Sperimentale (OGS)
Centro di Ricerche Sismologiche
Borgo Grotta Gigante 42/c
I-34010 Sgonico (Trieste)
Italy
pklin@inogs.it
epriolo@inogs.it
(P.K., E.P.)

Disaster Prevention Research Institute
Kyoto University
Gokasho, Uji
Kyoto 611-0011
Japan
iwaki@bosai.go.jp
iwata@egmdpri01.dpri.kyoto-u.ac.jp
(A.I., T.I.)

Université de Nice Sophia-Antipolis
Centre National de la Recherche Scientifique (CNRS)
IRD, Observatoire de la Côte d'Azur
GEOAZUR, UMR 7329
Sophia-Antipolis
F-06560 Valbonne
France
vincent.etienne@aramco.com
(V.E.)

Bureau des Recherches Géologiques et Minières (BRGM)
Direction Risques et Prévention
Unité Risques Sismique et Volcanique
3 avenue Claude Guillemin
BP 36009
F-45060 Orléans CEDEX 2
France
f.demartin@brgm.fr
(F.D.)

Institute of Engineering Seismology & Earthquake Engineering (ITSAK-EPPO)
P.O. Box 53 Finikas
GR-55102 Thessaloniki
Greece
ntheo@itsak.gr
(N.P.T.)

Aristotle University of Thessaloniki
P.O. Box 424
GR-54124 Thessaloniki
Greece
manakou@civil.auth.gr
kpitilak@civil.auth.gr
(M.M., K.P.)

Manuscript received 29 July 2014;
Published Online 19 May 2015